



HAL
open science

Methane thermometry in deep-sea hydrothermal systems: Evidence for re-ordering of doubly-substituted isotopologues during fluid cooling

Jabrane Labidi, E.D. Young, T. Giunta, I.E. Kohl, J. Seewald, H. Tang, M.D. Lilley, G.L. Früh-Green

► To cite this version:

Jabrane Labidi, E.D. Young, T. Giunta, I.E. Kohl, J. Seewald, et al.. Methane thermometry in deep-sea hydrothermal systems: Evidence for re-ordering of doubly-substituted isotopologues during fluid cooling. *Geochimica et Cosmochimica Acta*, 2020, 288, pp.248-261. 10.1016/j.gca.2020.08.013 . hal-03089851

HAL Id: hal-03089851

<https://hal.science/hal-03089851>

Submitted on 29 Dec 2020

HAL is a multi-disciplinary open access archive for the deposit and dissemination of scientific research documents, whether they are published or not. The documents may come from teaching and research institutions in France or abroad, or from public or private research centers.

L'archive ouverte pluridisciplinaire **HAL**, est destinée au dépôt et à la diffusion de documents scientifiques de niveau recherche, publiés ou non, émanant des établissements d'enseignement et de recherche français ou étrangers, des laboratoires publics ou privés.

1 **Methane thermometry in deep-sea hydrothermal systems: evidence for re-ordering of doubly-**
2 **substituted isotopologues during fluid cooling**

3 J Labidi^{1,2}, E D Young¹, T Giunta^{3,4}, I E Kohl^{1,5}, J Seewald⁶, H. Tang¹, M D Lilley⁷, G L Früh-Green⁸

4

5 ¹Department of Earth, Planetary, and Space Sciences, UCLA, Los Angeles, CA, USA.

6 ²Université de Paris, Institut de physique du globe de Paris, CNRS, Paris, France.

7 ³IFREMER, Unité des Géosciences Marines, 29280 Plouzané, France

8 ⁴Université de Bretagne Occidentale, Laboratoire Géosciences Océan, 29280 Plouzané, France

9 ⁵Thermo Fisher Scientific, Bremen, Germany.

10 ⁶Marine Chemistry and Geochemistry Department, Woods Hole Oceanographic Institution, Woods Hole, MA, USA.

11 ⁷School of Oceanography, University of Washington, Seattle USA.

12 ⁸Department of Earth Sciences, Eidgenössische Technische Hochschule Zurich (ETH-Z), Zurich, Switzerland.

13

14

15 **Abstract**

16 Deep-sea hydrothermal fluids are often enriched in carbon dioxide, methane, and hydrogen. Methane
17 effuses from metal-rich black smokers such as the Rainbow hydrothermal field, at temperatures higher than
18 200 °C. At the Lost City field, CH₄ emanates from alkaline fluids at < 100 °C. The abundance of the rare, mass-
19 18 CH₄ isotopologues, ¹³CH₃D and ¹²CH₂D₂, can mitigate degeneracies in the conventional isotopic signatures
20 of methane. We studied the isotopologue compositions of methane from the Rainbow, Lucky Strike, Von Damm,
21 and Lost City hydrothermal fields. At Rainbow, where the vented fluids are at ~360°C, our coupled Δ¹²CH₂D₂ -
22 Δ¹³CH₃D data establish that methane is in internal equilibrium at 343⁺⁴¹₋₃₅°C. This may track the formation
23 temperature of abiotic methane, or it may be the result of equilibration of methane isotopologues within the
24 carrier fluid. Lucky Strike and Von Damm have fluid temperatures < 300°C and although Δ¹³CH₃D values are
25 indistinguishable from those at Rainbow, ¹²CH₂D₂ abundances are marginally higher. At Lost City, Δ¹³CH₃D data
26 show a range of values, which at face value correspond to apparent temperatures of between 265⁺²⁸₋₂₄°C and

27 158^{+16}_{-14} °C, far hotter than fluid temperatures. A unique aspect of the Lost City data is the range of large $^{12}\text{CH}_2\text{D}_2$
28 excesses. The $\Delta^{12}\text{CH}_2\text{D}_2$ data correspond to temperatures of between 101^{+9}_{-8} °C and 69^{+4}_{-4} °C, showing a near-
29 perfect match with fluid temperatures. We find that mixing scenarios involving microbial methane may not
30 account for all of the isotope data. We suggest that $\Delta^{12}\text{CH}_2\text{D}_2$ values, unlike $\Delta^{13}\text{CH}_3\text{D}$ values, are prone to near-
31 complete re-equilibration at host fluid temperatures. We suggest that $^{13}\text{CH}_3\text{D}$ isotopologue data are consistent
32 with abiotic methane being synthesized at ~ 350 °C. On the other hand, $^{12}\text{CH}_2\text{D}_2$ isotopologue ordering records
33 post formation residence temperatures. We explore a possible mechanism decoupling the re-equilibration
34 systematics of the doubly-substituted isotopologues.

35

36 **1. Introduction**

37 Deep-sea hydrothermal fluids host mantle-derived CO₂ and various forms of reduced carbon that include
38 methane, C₂₊ alkanes, formate, and a variety of unsaturated molecules (Charlou et al., 2000; Charlou et al., 2002;
39 Charlou et al., 2010; Holm and Charlou, 2001; Konn et al., 2009; Lang et al., 2010; McDermott et al., 2015; Reeves
40 et al., 2014; Welhan, 1988; Welhan and Craig, 1979). So-called 'black smokers' vent hydrothermal fluid with
41 exit temperatures >300 °C and show significant amounts of molecular hydrogen (Fig. 1), which may allow for
42 the abiotic reduction of CO and/or CO₂ to methane (Berndt et al., 1996; Horita and Berndt, 1999; Jones et al.,
43 2010; McCollom, 2013; McCollom, 2016; McCollom et al., 2010; McCollom and Seewald, 2001; Neubeck et al.,
44 2011; Okland et al., 2014; Oze et al., 2012; Seewald et al., 2006). In the laboratory, abiotic methane formation
45 is sluggish (McCollom and Seewald, 2007) but may be enhanced by the presence of a catalyst, typically a Fe-Ni
46 alloy, preferably in the presence of H₂ vapor (McCollom, 2013; McCollom, 2016; McCollom et al., 2010). In
47 natural hydrothermal systems, the synthesis of abiotic methane may rather be catalyzed by oxides present in
48 mafic and ultramafic rocks (Foustoukos and Seyfried, 2004) during serpentinization. However, it is unclear
49 whether natural fluids are saturated in vapor (Welhan, 1988, Charlou et al. 2010). Whether they offer a set of
50 conditions allowing the rapid conversion of oxidized carbon to methane remains debated. Secondary fluid
51 inclusions may be an alternative source of abiotic methane: worldwide oceanic peridotites and gabbros host
52 vapor H₂- and CH₄-rich secondary fluid inclusions (Grozeva et al., 2020; Kelley and Früh-Green, 1999; Klein et
53 al., 2019). Within the inclusions, a complex interplay of reactions between olivine, oxidized carbon and gaseous
54 H₂ can lead to the synthesis of methane. As a result, inclusions contain up to 50 mole percent CH₄ (Grozeva et
55 al., 2020; Kelley, 1996; Kelley and Früh-Green, 1999; Klein et al., 2019) and could be a large reservoir where
56 abiotic methane formation occurs at temperatures below 340 °C by reduction of trapped magmatic CO₂ (Klein
57 et al. 2019, McDermott et al. 2015, Grozeva et al. 2020). Dissolution or fracturing of the olivine that hosts the
58 inclusions could simply release abiotic methane in hot hydrothermal fluids, like at Von Damm or Rainbow sites
59 (Klein et al., 2019; McDermott et al., 2015). Regardless of the exact process of abiotic methane synthesis, it
60 appears associated specifically with high temperature fluid-rock interaction in deep-sea hydrothermal
61 systems.

62 In contrast to high temperature black-smoker vents, hot-springs venting at the Lost City hydrothermal field
63 are characterized by considerably lower temperatures. However, Lost City fluids contain relatively high CH₄
64 and H₂ concentrations (Fig. 1), with isotopic and chemical signatures that are consistent with alkane
65 abiogenesis (Lang et al., 2012; Proskurowski et al., 2008), similar to observations made in hotter fluids
66 (McDermott et al., 2015). It is unclear whether fluids at Lost City record high-temperature events
67 (Proskurowski et al., 2006) and subsequently underwent conductive cooling, or if low-temperature chemistry
68 allowed the synthesis of abiotic alkanes. A complication is that the coldest vents at Lost City (T < 60°C) host
69 biofilms containing 10⁶-10⁹ cells per gram of carbonate, dominated by the Lost City *Methanosarcinales*
70 (Brazelton et al., 2006; Kelley et al., 2005; Schrenk et al., 2004). These methanogens may contribute methane
71 to the fluids at those vents (Bradley and Summons, 2010) and the contribution

72 The concentrations of the mass-18 isotopologues of methane, ¹³CH₃D and ¹²CH₂D₂, can elucidate the origins
73 and thermal histories of methane gases in hydrothermal fields. In Δ¹³CH₃D versus Δ¹²CH₂D₂ space (Figure 2),
74 ¹³CH₃D/¹²CH₄ and ¹²CH₂D₂/¹²CH₄ ratios are reported relative to the stochastic distribution of isotopologues. In
75 this diagram, methane in thermodynamic equilibrium with respect to isotopologue abundances falls on an
76 equilibrium curve, where the relative abundances of rare isotopologues yield concordant temperatures (Figure
77 2). When equilibrium signatures are observed, the assumption that methane isotopologue may constrain CH₄
78 thermometry (Stolper et al. 2014) may be valid (Young et al., 2017). In laboratory experiments, both biotic and
79 abiotic methane exhibits disequilibrium deficits of ¹²CH₂D₂ at varying Δ¹³CH₃D values (Giunta et al. 2019,
80 Young et al. 2017). In the case of microbial methane, kinetic controls result in anomalously low values for both
81 Δ¹²CH₂D₂ and Δ¹³CH₃D relative to formation-temperature estimates (Wang et al. 2015, Young et al. 2017). Such
82 signatures were observed in sedimentary and lacustrine settings (Young et al. 2017, Giunta et al. 2019, Young
83 2019). Alternatively, partial reversibility of key enzymatic reactions during microbial methanogenesis (Stolper
84 et al., 2015; Wang et al., 2015) and/or syntrophic microbial mediation (Ash et al., 2019; Giunta et al., 2019;
85 Young et al., 2017; Young, 2019) could lead to biogenic methane characterized by equilibrium abundances of
86 CH₄ isotopologues. Abiotic methane may exhibit peculiar signatures at high temperatures (Young et al. 2017);
87 the few experimental data suggest Δ¹³CH₃D may preserve CH₄ formation temperatures of abiotic methane,
88 while Δ¹²CH₂D₂ can exhibit substantial depletions qualitatively similar to those produced by microbial

89 methanogenesis. This pronounced abiotic disequilibrium in $\Delta^{12}\text{CH}_2\text{D}_2$ values is well illustrated by methane in
90 $\sim 25^\circ\text{C}$ fluids from the Kidd Creek mine, where CH_4 has been suggested to be abiotic in origin (Sherwood Lollar
91 et al., 1993; Sherwood Lollar et al., 2006; Sherwood Lollar et al., 2002). There, $\Delta^{13}\text{CH}_3\text{D}$ values are broadly
92 consistent with environmental temperatures in the mine and inferred temperatures of methane formation
93 (Young et al. 2017; Sherwood Lollar et al. 2002) while remarkable $\Delta^{12}\text{CH}_2\text{D}_2$ depletions of up to $\sim 25\%$ relative
94 to equilibrium are observed (Young et al. 2017). Although the $\Delta^{12}\text{CH}_2\text{D}_2$ formation temperatures are lost in this
95 case, the disequilibrium isotopologue signature may be a diagnostic feature of abiotic methanogenesis (Young
96 et al. 2017; Young 2019). Based on these burgeoning but still unclear signatures of methane formation
97 pathways, methane isotopologues may provide new constraints on the origin and/or the thermal history of CH_4
98 in hydrothermal vent settings.

99 Wang et al. (2018) published the first $\Delta^{13}\text{CH}_3\text{D}$ methane isotopologue data for deep-sea hydrothermal fields.
100 At Rainbow, Lucky Strike, Von Damm, and Lost City, they measured a homogenous $\Delta^{13}\text{CH}_3\text{D}$ values of
101 $\sim 1.6 \pm 0.3\%$. This value suggests a temperature of $^{13}\text{CH}_3\text{D}$ ordering of $310_{-42}^{+53}\text{ }^\circ\text{C}$, indicating abiotic methane
102 formed at high-temperatures contributes to all studied hydrothermal fluids, including the fluids at Lost City
103 (Wang et al., 2018). Because the homogeneous $\Delta^{13}\text{CH}_3\text{D}$ is observed for fluids with varying exit temperatures
104 (between 370 and 96°C), it was suggested that $\Delta^{13}\text{CH}_3\text{D}$ ordering is preserved upon fluid cooling (Wang et al.
105 2018). An original aspect of the clumped CH_4 systematics is that two doubly-substituted isotopologues can be
106 measured independently (Young et al. 2016). Coupling these two species may help constrain the thermal
107 history of methane. A current unknown is the relative behavior of $\Delta^{12}\text{CH}_2\text{D}_2$ compared to $\Delta^{13}\text{CH}_3\text{D}$ in
108 hydrothermal fluids containing methane. It is unclear whether $\Delta^{12}\text{CH}_2\text{D}_2$ may provide new constraints on the
109 origin of CH_4 in hot hydrothermal fluids. If so, we predict disequilibrium $\Delta^{12}\text{CH}_2\text{D}_2$ signatures will help track
110 abiotic methane in natural samples, similar to signatures observed in the $\sim 25^\circ\text{C}$ fluids at the Kidd Creek mine
111 (Young et al. 2017). Alternatively, any $\Delta^{12}\text{CH}_2\text{D}_2$ abiotic signature may be erased at elevated temperatures, via
112 re-ordering of $^{12}\text{CH}_2\text{D}_2$ isotopologue. It is unclear whether $\Delta^{13}\text{CH}_3\text{D}$ would also be affected by re-ordering at all.
113 In other words, potential re-ordering processes may cloud the meaning of the CH_4 systematics. In the absence
114 of experimental data on the behaviors of $\Delta^{12}\text{CH}_2\text{D}_2$ and $\Delta^{13}\text{CH}_3\text{D}$ in hot fluids, we present data of $\Delta^{13}\text{CH}_3\text{D}$ and

115 $\Delta^{12}\text{CH}_2\text{D}_2$ measured in gases from deep-sea hydrothermal fluids sampled at Lucky Strike, Rainbow, Von Damm
116 and Lost City. These fluids experienced variable extents of conductive cooling, allowing a test of whether
117 $\Delta^{13}\text{CH}_3\text{D}$ and $\Delta^{12}\text{CH}_2\text{D}_2$ may be re-ordered in natural fluids. Ultimately, the data are used to examine how
118 $\Delta^{13}\text{CH}_3\text{D}$ and $\Delta^{12}\text{CH}_2\text{D}_2$ may constrain the origin and/or the thermal evolution of methane in hydrothermal
119 systems. Some of our samples are the same aliquots of gas analyzed for $\Delta^{13}\text{CH}_3\text{D}$ by laser spectroscopy by Wang
120 et al. (2018), to which we add the first $\Delta^{12}\text{CH}_2\text{D}_2$ measurements. For Lost City, $\Delta^{13}\text{CH}_3\text{D}$ and $\Delta^{12}\text{CH}_2\text{D}_2$
121 measurements are reported for four new samples. Our samples from all of the sites span a large range of
122 measured vent temperatures, from 65 to 370°C. With these samples, we ascertain whether both mass-18
123 methane isotopologues record concordant temperatures of bond-ordering or if they record distinctive aspects
124 of methane thermal history.

125

126 **2. Samples and geological context**

127 Rainbow is a hydrothermal field hosted in ultramafic rocks at 36°14' N on the Mid-Atlantic ridge (MAR), at
128 a water depth of 2300 meters (Charlou et al., 2002; Seyfried Jr et al., 2011). At Rainbow, hydrothermal fluids
129 have temperatures up to 370 °C and are the hottest fluids studied here. Hydrothermal fluids show chloride
130 concentrations significantly higher than seawater, indicative of a brine-vapor phase separation occurring at
131 depth at a minimum temperature of 380 °C (Charlou et al. 2002). The hydrothermal endmember contains ~2
132 mM CH_4 (Fig. 1) with a $\delta^{13}\text{C}$ of ~-15‰ (Charlou et al. 2002; Seyfried et al., 2011).

133 Lucky Strike is an unsedimented hydrothermal vent field hosted in basaltic rock, at 37°17' N on the MAR,
134 with fluid temperatures up to 324 °C (Charlou et al., 2000; Pester et al., 2012). Lucky Strike is a relatively
135 shallow system with a seafloor depth of 1700 meters. There, the vent fluids have low silica, metal and rare earth
136 content and are thought to reflect a rapid upflow of fluids to the surface with short water-rock reaction times
137 (Charlou et al., 2000). Chloride concentration of hydrothermal fluids at Lucky Strike indicate the circulating
138 seawater experienced brine-vapor phase separation at $T > 360^\circ\text{C}$, but at relatively low-pressure (Charlou et al.
139 2000). The methane concentration at Lucky Strike is ~1mM (Fig. 1) with a $\delta^{13}\text{C}$ of ~-13‰ (Charlou et al. 2000;
140 Pester et al., 2012).

141 The Von Damm site at 18°22' N on the Mid-Cayman rise is hosted in ultramafic, gabbroic, and basaltic rocks,
142 at 2350 meters below seafloor (Connelly et al., 2012). There, hydrothermal fluids emanate at temperatures as
143 high as 226 °C (McDermott et al., 2015). Evidence that fluids experienced phase separation at Von Damm is
144 inconclusive (McDermott et al. 2015). Methane concentration in the hydrothermal endmember is ~ 3mM CH₄
145 (Fig. 1) with a δ¹³C of ~-15‰ (McDermott et al. 2015). For all high-temperature hydrothermal fields, δD data
146 for CH₄ are scarce. To date, only Wang et al. (2018) published δD values for the studied sites, with all samples
147 yielding values around -110±15‰. These values are consistent with a D/H equilibrium between methane and
148 water established during methane formation, at ~300 °C (Wang et al. 2018), based on the experimental data
149 from Horibe and Craig (1995).

150 Lost City is located ~15 km west of the Mid-Atlantic Ridge in 1.5 my old lithosphere dominated by ultramafic
151 rocks with minor mafic intrusions that have been exposed through detachment faulting. It is a serpentinite-
152 hosted hydrothermal system, venting relatively cool (20–100 °C) fluids. In contrast with other systems studied
153 here that vent acidic fluids, Lost City is the only field venting highly alkaline fluids with pH values > 9 (Kelley et
154 al., 2001; Kelley et al., 2005). The lower temperatures at LCHF may be due to the location of the site, a few
155 kilometers off the mid-Atlantic ridge axis and thus not directly above a localized heat source. The chlorinity of
156 Lost City fluid is similar to seawater, suggesting no brine separation occurred beneath the Lost City
157 hydrothermal field (Allen and Seyfried Jr, 2004). This is generally consistent with thermodynamic modelling
158 suggesting maximum temperatures of 200±50°C (Foustoukos et al., 2008; Seyfried Jr et al., 2015) although in
159 the past mantle rocks in the Lost City basement experienced a higher-temperature alteration history (Früh-
160 Green et al., 2018; Rouméjon et al., 2018). Maximum temperatures of 200±50°C for fluids currently circulating
161 in the system appear to be lower than at the other sites, but the much cooler effusion temperatures of < 100°C
162 nonetheless suggest that circulating fluids at Lost City underwent significant conductive cooling prior to
163 venting.

164 Samples from Rainbow and Lucky Strike were collected by ROV Jason II during cruises to the Mid-Atlantic
165 Ridge in 2008 (Pester et al., 2012; Reeves et al., 2014; Seyfried Jr et al., 2011). Rainbow samples are from three
166 vents: *Guillaume*, *Auberge*, and *CMSP_and_P* (all venting at 365±10°C). The sample from Lucky Strike is from
167 the vent *Isabel* (venting at 292 °C). Samples from Von Damm were collected on the Mid-Cayman Rise in 2012
168 (McDermott et al., 2015). They are from two vents, *East Summit* (226°C) and *Ravelin* (145°C) and ~~*Old Man Tree*~~

169 (115°C). Six Lost City samples were collected during the 2008 ROV Jason II cruise (J2-361-IGT5), the 2005 Lost
170 City expedition (H06_GT_15/16) and the 2018 cruise to Lost City (J2-1107-GT9, J2-1111-Titan, J2-1110-GT18,
171 J2-1110-Titan). They are from three vents: *Beehive* ($\sim 100^{\circ}\text{C}$), *Marker C* ($\sim 85^{\circ}\text{C}$), and *Marker 2* ($\sim 65^{\circ}\text{C}$). Eight
172 of our samples were previously analyzed by laser spectroscopy at MIT (Wang et al. 2018). Those were from
173 Rainbow (n=3), Von Damm (n=3), Lucky Strike (n=3) and Lost City (*Beehive* only, n=1). The six remaining
174 samples were not analyzed previously for either methane bulk isotope compositions nor for the rarer mass-18
175 methane isotopologues.

176 Due to near-zero concentrations of dissolved magnesium (Mg) in endmember hydrothermal vent fluids,
177 measured Mg concentrations in sampled fluids can be used to estimate the extent of seawater entrainment
178 during sampling or subsurface mixing. Concentrations of dissolved CH_4 concentrations plotted against
179 dissolved Mg concentration for fluids from all sites studied are shown in Figure 1 with data from the literature
180 (Reeves et al. 2014; McDermott et al. 2015). Despite the considerable mixing shown in Figure 1, we picked
181 samples from Lucky Strike, Lost City, and Rainbow with low Mg concentration that can be considered to have
182 minimal seawater contribution from sampling and thus more representative of the hydrothermal endmember.
183 In contrast, based on Mg concentration reported in the literature, subseafloor seawater mixing before
184 discharge occurred in some of the samples from Von Damm. One of our samples from a central vent (*Summit*)
185 is devoid of seawater contamination and represents the local hydrothermal endmember, at 226°C , while the
186 other (*Ravelin*) shows evidence for subseafloor mixing with seawater that is reflected by a lower exit
187 temperature of 145°C (McDermott et al., 2015).

188

189 3. Measurement protocol

190 Methane was extracted from breakseals on a vacuum system at UCLA and purified by gas
191 chromatography using procedures described previously by Young et al. (2017). Between 40 and 120
192 micromoles of methane were available for each sample in our study (Table 1). Gases analyzed previously at
193 MIT were subsequently trapped onto silica gel and sealed in quartz tubes for storage and transport to UCLA. At
194 UCLA, the vacuum-line with a resting pressure of 3×10^{-5} mbar or lower was used to purify the samples. The

195 gases were transferred from the breakseals into a silica gel-filled stainless-steel u-trap cooled with liquid
196 nitrogen. Helium carrier gas was used to flush the sample to the gas chromatograph. Separation was
197 accomplished with a 3m long, 1/8 in. OD stainless steel column packed with 5 A molecular sieve, followed in
198 series by a 2m long 1/8 in. OD stainless steel column packed with HayeSep D porous polymer. Gas
199 chromatograph peaks were detected with an in-line, passive thermal conductivity detector (TCD). Once
200 methane collection was complete, methane was transferred to a glass vial filled with silica-gel at liquid nitrogen
201 temperature and subsequently connected to the inlet of the Panorama mass spectrometer where it was
202 warmed and expanded into the mass spectrometer.

203 Isotopologue measurements were made using the Panorama instrument, a Matsuda-type large radius
204 high-resolution mass spectrometer at UCLA with a mass resolving power that allows the simultaneous
205 measurement of ion currents for resolved $^{12}\text{CH}_4^+$, $^{13}\text{CH}_4^+$, $^{12}\text{CH}_3\text{D}^+$, $^{13}\text{CH}_3\text{D}^+$ and $^{12}\text{CH}_2\text{D}_2^+$ ion beams. The
206 measured ratios of these ion currents yield values for both $\Delta^{13}\text{CH}_3\text{D}$ and $\Delta^{12}\text{CH}_2\text{D}_2$ as well as for bulk $^{13}\text{C}/^{12}\text{C}$
207 and D/H. The mass spectrometer is set to a mass resolving power equal to or greater than 40,000. Both low
208 abundances of the mass-18 isotopologues, $^{13}\text{CH}_3\text{D}^+$, and $^{12}\text{CH}_2\text{D}_2^+$, require that measurements are made with an
209 electron multiplier. Isotopologues of masses 16 and 17 are measured on Faraday collectors with amplifier
210 resistors of $10^{11} \Omega$. The bulk carbon and hydrogen stable isotopic ratios are reported relative to the
211 international standards V- PDB and V-SMOW, respectively, and expressed in permil units using the delta
212 notation:

$$213 \quad \delta^{13}\text{C} = \left[\frac{(^{13}\text{C}/^{12}\text{C})_{\text{sample}}}{(^{13}\text{C}/^{12}\text{C})_{\text{VPDB}}} - 1 \right] \times 1000 \quad (1)$$

214 and

$$215 \quad \delta\text{D} = \left[\frac{(\text{D}/\text{H})_{\text{sample}}}{(\text{D}/\text{H})_{\text{VSMOW}}} - 1 \right] \times 1000 \quad (2).$$

216

217 Mass-18 isotopologue compositions are reported versus a stochastic distribution expressed in permil using the
218 capital delta notation:

219

$$220 \quad \Delta^{13}\text{CH}_3\text{D} = \left[\frac{(^{13}\text{CH}_3\text{D}/^{12}\text{CH}_4)_{\text{sample}}}{(^{13}\text{CH}_3\text{D}/^{12}\text{CH}_4)_{\text{stochastic}}} - 1 \right] \times 1000 \quad (3)$$

221 and

$$\Delta^{12}\text{CH}_2\text{D}_2 = [({}^{12}\text{CH}_2\text{D}_2/{}^{12}\text{CH}_4)_{\text{sample}}/({}^{12}\text{CH}_2\text{D}_2/{}^{12}\text{CH}_4)_{\text{stochastic}} - 1] \times 1000 \quad (4).$$

223

224 The relationship between $\Delta^{13}\text{CH}_3\text{D}$ and $\Delta^{12}\text{CH}_2\text{D}_2$ and temperature has been predicted through *ab initio*
225 calculations and can be represented by the following expressions (Young et al., 2017):

226

$$\Delta^{13}\text{CH}_3\text{D} (T) \approx 1000 \ln (1 + 0.0355502/T - 433.038/T^2 + 1270210.0/T^3 - 5.94804 \times 10^8/T^4 + 1.196630 \times 10^{11}/T^5 - 9.07230 \times 10^{12}/T^6) \quad (5)$$

229 and

$$\Delta^{12}\text{CH}_2\text{D}_2 (T) \approx 1000 \ln (1 + 0.183798/T - 785.483/T^2 + 1056280.0/T^3 + 9.37307 \times 10^7/T^4 - 8.919480 \times 10^{10}/T^5 + 9.901730 \times 10^{12}/T^6) \quad (6)$$

232

233 where T is in Kelvin. These equations were verified using methane samples equilibrated over a range of
234 temperatures in the UCLA laboratory (Young et al. 2017) and are consistent with gases equilibrated at low
235 temperatures in other laboratories (Eldridge et al. 2019, Wang et al. 2019). Equations (5) and (6) show that
236 when methane is formed at thermodynamic equilibrium, $\Delta^{13}\text{CH}_3\text{D}$ and $\Delta^{12}\text{CH}_2\text{D}_2$ are both positive, and must
237 approach 0‰ at high temperatures (>1000 K).

238 Variable volume bellows for the sample and reference gases are adjusted after each measurement cycle
239 of approximately 30 seconds so that ion current intensities are always balanced during the analyses. The mass
240 spectrometry integration methods are described in Young et al. (2016). For standards and samples available in
241 quantities > 80 μmol , relative abundances of ${}^{13}\text{CH}_3\text{D}^+$ and ${}^{12}\text{CH}_2\text{D}_2^+$ are measured for up to 10 and 20 hours,
242 respectively. In these cases, typical propagated internal errors for the calculation of $\Delta^{13}\text{CH}_3\text{D}$ and $\Delta^{12}\text{CH}_2\text{D}_2$ are
243 generally $\pm 0.1\%$ and $\pm 0.5\%$, respectively. The external reproducibility is estimated based on repeated
244 measurements of the thermogenic Utica shale gas, done with $\sim 80 \mu\text{mol}$ of CH_4 . Eight standards were measured
245 over the course of this study (Supplementary table 1), yielding average $\delta^{13}\text{C}$ and δD values of $-25.81 \pm 0.06\%$
246 and $-154.0 \pm 0.1\%$, and average $\Delta^{13}\text{CH}_3\text{D}$ and $\Delta^{12}\text{CH}_2\text{D}_2$ values of $2.8 \pm 0.1\%$ and $8.8 \pm 0.8\%$ (all 1 s.d.). In our
247 study, often only 40 to 60 μmol of CH_4 were available (Table 1), and uncertainties are larger, reflecting less

248 favorable counting statistics. The internal uncertainties range from 0.2‰ and 0.5‰ for $\Delta^{13}\text{CH}_3\text{D}$, and between
249 0.5‰ and 2.7‰ for $\Delta^{12}\text{CH}_2\text{D}_2$. Note that for all samples except two gases from Von Damm that yielded the
250 smallest CH_4 quantities of the sample set, the internal uncertainties remained below 0.3‰ for $\Delta^{13}\text{CH}_3\text{D}$, and
251 1.0‰ for $\Delta^{12}\text{CH}_2\text{D}_2$.

252

253 4. Results

254 Our bulk isotope ratios are in general agreement with previously-published CH_4 isotopic data for these
255 localities (Charlou et al., 2002, Seyfried et al., 2011, 2015; Pester et al., 2012; McDermott et al., 2015; Wang et
256 al., 2018, Proskurowski et al., 2008). In δD vs $\delta^{13}\text{C}$ space the samples plot in the ^{13}C - and D- enriched extremity
257 of the abiotic methane field (Fig. 3) (Etiope and Sherwood Lollar, 2013). Comparison with the data of Wang et
258 al. (2018) shows good agreement. Disagreement is found for one datum for sample J2-612-IGT2 from Von
259 Damm where there is a discrepancy in δD between the two laboratories, with the UCLA value being lower by
260 $\sim 5\text{‰}$. The UCLA datum for this sample also exhibit a low $\delta^{13}\text{C}$ value relative to the MIT value, consistent with
261 a 1:10 $\delta^{13}\text{C}$ - δD fractionation that must have occurred between the moment it was measured at MIT and the
262 moment it was measured at UCLA. We speculate that a fractionation could have occurred during incomplete
263 sample freezing onto the silica gel in the quartz tube at MIT. Nonetheless, we determined a $\Delta^{13}\text{CH}_3\text{D}$ value from
264 this gas that is indistinguishable from that reported by Wang et al. (2018), within uncertainties. This suggests
265 that if a fractionation had occurred during the trapping of the sample at MIT, or during gas processing at UCLA,
266 it was not sufficient to affect the apparent bond ordering.

267 Our methane isotopologues results (Table 1, Fig. 2) yield values of $\Delta^{13}\text{CH}_3\text{D}$ between 1.0 ± 0.2 and $3.0\pm 0.2\text{‰}$,
268 expanding the range of 1.0 ± 0.6 to $1.9\pm 0.3\text{‰}$ reported by Wang et al. (2018) for deep-sea hydrothermal vent
269 systems. No direct relationship is observed between the UCLA and MIT values, because of the narrow spread
270 of the eight samples measured in both laboratories, and because of the relative uncertainties. For the first time,
271 we report $\Delta^{12}\text{CH}_2\text{D}_2$ values for deep-sea hydrothermal methane, and we show the samples have values ranging
272 from $1.7\pm 1.0\text{‰}$ to $11.6\pm 0.5\text{‰}$ (Table 1, Fig. 2). No $\Delta^{12}\text{CH}_2\text{D}_2$ values below zero are observed, in contrast with

273 measurements of putative abiotic methane from the Kidd Creek mine (Young et al. 2017). Within analytical
274 uncertainties, isotopologue abundances in samples from Rainbow are consistent with internal equilibrium with
275 the ambient fluids (Fig. 2), with average $\Delta^{13}\text{CH}_3\text{D}$ and $\Delta^{12}\text{CH}_2\text{D}_2$ values of $1.4\pm 0.2\text{‰}$ and $2.7\pm 0.9\text{‰}$ ($n=3$, both
276 1 s.d.), respectively. Samples from Lucky Strike and Von Damm show similar signatures, with $\Delta^{13}\text{CH}_3\text{D}$ data
277 ranging from $1.0\pm 0.2\text{‰}$ to $1.7\pm 0.4\text{‰}$, and $\Delta^{12}\text{CH}_2\text{D}_2$ values that are slightly higher than values at Rainbow. At
278 Von Damm, $\Delta^{12}\text{CH}_2\text{D}_2$ values are $+4.4\pm 1.0\text{‰}$ and $4.5\pm 1.8\text{‰}$ for *Ravelin* and *Summit* vents, respectively. In
279 contrast, gases from Lost City are characterized by disequilibrium isotopologue signatures (Fig. 2). The Lost
280 City samples exhibit $\Delta^{13}\text{CH}_3\text{D}$ values between $1.9\pm 0.2\text{‰}$ and $3.0\pm 0.2\text{‰}$ extending the range of values
281 previously known for Lost City (Wang et al., 2018). $\Delta^{12}\text{CH}_2\text{D}_2$ values are between $10.7\pm 0.9\text{‰}$ and $14.5\pm 1.0\text{‰}$.
282 The highest values are observed in *Marker 2*, the coolest vent, while *Beehive* and *Marker C* show consistent
283 compositions. All methane from Lost City plots far above the equilibrium curve in $\Delta^{13}\text{CH}_3\text{D}$ vs. $\Delta^{12}\text{CH}_2\text{D}_2$ space.
284 We find no relationships between the isotopologue signatures and host rock (whether hydrothermal fluids are
285 hosted in basaltic versus ultramafic rocks), seafloor depth, or likely maximal pressures reached in the
286 subsurface (Fig. 2). We argue below that the isotopologue signatures result from partial or near-complete re-
287 equilibration of doubly-substituted isotopologues at environmental temperatures.

288

289 5. Discussion

290 5.1. Equilibrium signatures for methane isotopologues

291 The methane isotopologue data for the hydrothermal systems studied here show signatures ranging from
292 equilibrium to disequilibrium, from the hottest to the coldest fluids, respectively (Fig. 2). Samples from
293 Rainbow have average $\Delta^{13}\text{CH}_3\text{D}$ and $\Delta^{12}\text{CH}_2\text{D}_2$ values that represent thermodynamic equilibrium among the
294 methane isotopologues. The $\Delta^{13}\text{CH}_3\text{D}$ values correspond to an apparent temperature of 343^{+41}_{-35} °C, similar to
295 that derived previously (Wang et al. 2018). The temperature indicated by the $\Delta^{12}\text{CH}_2\text{D}_2$ values is 334^{+78}_{-53} °C,
296 indistinguishable from that derived from the more abundant $^{13}\text{CH}_3\text{D}$ isotopologue, albeit less precise. This
297 establishes that methane from Rainbow is in isotopic bond-ordering equilibrium.

298 Equilibrium could result from abiotic methane synthesis. This would be in contrast with deficits in $\Delta^{12}\text{CH}_2\text{D}_2$
299 where abiotic methanogenesis may have occurred at low temperatures at the Kidd Creek mine, where fluids
300 carrying methane show measured temperatures of $\sim 25^\circ\text{C}$ (Sherwood Lollar et al., 2002, Young et al., 2017).
301 Equilibrium signatures in hot fluids could alternatively represent re-equilibration at high temperatures rather
302 than being the result of the formation mechanism. Re-ordering is also suspected because disequilibrium
303 $\Delta^{12}\text{CH}_2\text{D}_2$ signatures seem to be associated with abiotic CH_4 formation in laboratory experiments with
304 durations from 12 to 30 days (Young et al., 2017). The few data for abiotic methane synthesized experimentally
305 suggest $\Delta^{13}\text{CH}_3\text{D}$ -based temperatures to be roughly consistent with experimental temperatures of abiotic CH_4
306 formation, while $\Delta^{12}\text{CH}_2\text{D}_2$ depletions of ~ 2 to 60% relative to equilibrium were observed between 75 and 500
307 $^\circ\text{C}$. Only experiments where methane was synthesized at 600°C during about 12 days yielded equilibrium for
308 both $\Delta^{12}\text{CH}_2\text{D}_2$ and $\Delta^{13}\text{CH}_3\text{D}$ values (Young et al. 2017). We emphasize that it is unlikely that the experiments
309 presented in Young et al. (2017) are an accurate representation of geochemical processes in deep-sea
310 hydrothermal fields. It is interesting, however, that the two sets of experiments explored different formation
311 mechanisms, the Fischer-Tropsch-type Sabatier reaction and silane hydration, and yielded broadly consistent
312 results. In the silane experiments, $\text{Si}_5\text{C}_{12}\text{H}_{36}$ reacts with H_2O to produce SiO_2 , CH_4 and H_2 (Foustoukos and
313 Mysen, 2013) In the Sabatier processes, CO_2 is converted to CH_4 catalyzed with ruthenium at temperature $<$
314 100°C (Etiope and Ionescu, 2015). In both experiments, the large $\Delta^{12}\text{CH}_2\text{D}_2$ depletions may result from a
315 quantum tunneling effect expressed during hydrogenation of methane precursors (Young et al. 2017).
316 Alternatively, it may result from what is termed a “combinatorial effect” caused by mixing sources of hydrogen
317 with markedly different D/H produced by classical kinetic and equilibrium partitioning of isotopes associated
318 with the various hydrogenation steps during reduction of oxidized carbon (Cao et al., 2019; Young et al., 2017;
319 Young, 2019). Hydrogen with wide ranging D/H ratios is sourced from different reversible and irreversible
320 steps during methane formation, resulting in deficits in $\Delta^{12}\text{CH}_2\text{D}_2$ caused by mixing the various sources of
321 hydrogen (Röckmann et al., 2016; Taenzer et al., 2020; Yeung, 2016). The two mechanistic interpretations
322 described here both allow the preliminary experimental results from Young et al. (2017) to be extrapolated to
323 natural settings, but further experimental work is needed.

324 In the context of the limited natural and experimental evidence, we tentatively suggest that equilibrium
325 signatures at Rainbow (Fig. 2) might result from re-ordering rather than being inherited directly from abiotic
326 methane synthesis. Secondary fluid-inclusions in gabbroic and ultramafic rocks likely contribute abiotic
327 methane to hydrothermal fields (Kelley and Fruh Green, 1999, McDermott et al. 2015, McCollom, 2016, Klein
328 et al. 2019). The inclusions may also provide conditions suitable for post-formation re-equilibration, since they
329 contain metal oxides possibly contributing to catalysis (Klein et al. 2019, Grozeva et al. 2020) and would likely
330 host methane over long periods of time. Alternatively, the concordant temperatures may reflect a rapid re-
331 equilibration of all doubly-substituted isotopologues in the hot carrier fluid: at Rainbow, the $\Delta^{13}\text{CH}_3\text{D}$ -based
332 temperature of 343^{+41}_{-35} °C and the $\Delta^{12}\text{CH}_2\text{D}_2$ temperature of 334^{+78}_{-53} °C are both statistically indistinguishable
333 from the temperature of the carrier fluid ($360\pm 10^\circ\text{C}$). Our data are therefore consistent with abiotic methane
334 synthesis or re-equilibration in either the source fluid inclusions or in the carrier fluid at this site.

335 Methane from Lucky Strike and Von Damm show $\Delta^{13}\text{CH}_3\text{D}$ values similar to those at Rainbow, but display
336 marginally higher $\Delta^{12}\text{CH}_2\text{D}_2$ values. Our one sample from Lucky Strike (from the *Isabel* vent) is virtually devoid
337 of seawater contamination and is associated with a measured fluid temperature of 292 °C (Pester et al., 2012).
338 The $\Delta^{13}\text{CH}_3\text{D}$ values of $1.0\pm 0.2\text{‰}$ suggest a temperature of 430^{+60}_{-50} °C. The $\Delta^{12}\text{CH}_2\text{D}_2$ value of $+2.9\pm 0.7\text{‰}$
339 corresponds to an apparent temperature of 320^{+50}_{-39} °C. The latter estimate is within uncertainty of the measured
340 fluid temperature (Fig. 4). At Von Damm, fluids are venting at a maximum temperature of 226 °C, but many of
341 the fluids have experienced seafloor mixing with cold seawater and are thus characterized by vent
342 temperatures $< 226^\circ\text{C}$ (McDermott et al., 2015). The $\Delta^{13}\text{CH}_3\text{D}$ values are homogeneous and average $1.5\pm 0.2\text{‰}$
343 which yields an apparent temperature of 325^{+40}_{-31} °C. The $\Delta^{12}\text{CH}_2\text{D}_2$ values are homogeneous as well but with an
344 average of $\sim +4.5\pm 1.0\text{‰}$, corresponding to a lower temperature of 247^{+43}_{-35} °C, similar to the measured
345 hydrothermal maximum temperature of 226 °C (Fig. 4). We see no correlations between methane isotopologue
346 data and the extent of seafloor mixing with seawater (Table 1). The methane concentration of seawater is
347 so low that arguably, seawater contamination does not add significant amounts of methane to the bulk vent
348 fluid. We additionally conclude that both $\Delta^{13}\text{CH}_3\text{D}$ and $\Delta^{12}\text{CH}_2\text{D}_2$ values remain unaffected by the abrupt cooling
349 associated with seawater infiltration.

350 Based on these results, we suggest that the methane isotopologue data at Rainbow, Lucky Strike and Von
351 Damm are all consistent within 2σ with high-temperature methane formed at ~ 330 °C, as recorded by $\Delta^{13}\text{CH}_3\text{D}$.
352 This thermometry is consistent with methane originating from secondary fluid inclusions, where
353 thermodynamic modeling suggests it was synthesized over geological timescales at temperatures between 300
354 and 400°C (Klein et al., 2019). Our results also imply re-ordering of the original $\Delta^{12}\text{CH}_2\text{D}_2$ values in the cooler
355 carrier fluids. However, the $\Delta^{12}\text{CH}_2\text{D}_2$ re-ordering is about 2‰ and thus its detection is marginal given the
356 measurement uncertainties of $\sim 1\%$. We show below that data obtained on the coldest site studied here, Lost
357 City, are more dispositive with regard to the origin of discordance between $\Delta^{13}\text{CH}_3\text{D}$ and $\Delta^{12}\text{CH}_2\text{D}_2$ values.

358 5.2: Substantial $\Delta^{12}\text{CH}_2\text{D}_2$ re-equilibration or mixing in the cold Lost City fluids

359 Unlike at the other sites, at Lost City methane is carried to the seafloor by relatively cool fluids. The three
360 vents examined, *Beehive* (~ 100 °C), *Marker C* (~ 85 °C), and *Marker 2* (~ 65 °C), show much lower temperatures
361 than other vents studied here. The $\Delta^{13}\text{CH}_3\text{D}$ values are consistent with equilibration temperatures between
362 265^{+28}_{-24} °C and 158^{+16}_{-14} °C, far hotter than the measured fluid temperatures. The $\Delta^{12}\text{CH}_2\text{D}_2$ values yield
363 temperature estimates of 101^{+9}_{-8} °C, 93^{+9}_{-8} °C and 69^{+4}_{-4} °C, showing a near-perfect match with the vent fluid
364 temperatures (Fig. 4). The highest $\Delta^{13}\text{CH}_3\text{D}$ and $\Delta^{12}\text{CH}_2\text{D}_2$ values are observed in the coldest vent, *Marker 2*.
365 These discordant isotopologue temperatures constitute marked disequilibrium (Fig. 2).

366 Before discussing the evidence of $\Delta^{12}\text{CH}_2\text{D}_2$ re-ordering at Lost City, we consider first whether the
367 disequilibrium seen in the $\Delta^{13}\text{CH}_3\text{D}$ and $\Delta^{12}\text{CH}_2\text{D}_2$ data could be the result of mixing (e.g., Young et al., 2017). A
368 relatively constant $\text{CH}_4/{}^4\text{He}$ ratio observed in Lost City vent fluids argues in favor of a unique abiotic source
369 (Proskurowski et al. 2008, Lang et al. 2012). However, others have suggested a possible contribution from
370 biotic sources (Bradley et al. 2009, 2010); the coldest vents at Lost City ($T < 60$ °C) host biofilms dominated by
371 the Lost City *Methanosarcinales* phylotype (Brazelton et al., 2006; Kelley et al., 2005; Schrenk et al., 2004). The
372 methanogens may contribute significant microbial methane to the fluids at those vents (Bradley and Summons,
373 2010). In principle mixing between abiotic and microbial methane could account for the Lost City characteristic
374 excesses in $\Delta^{12}\text{CH}_2\text{D}_2$. Our use of two mass-18 isotopologues affords the ability to identify mixing if it occurred

375 at Lost City: mixing trajectories in $\Delta^{13}\text{CH}_3\text{D}$ versus $\Delta^{12}\text{CH}_2\text{D}_2$ space may trend above the equilibrium curve into
376 positive $\Delta^{12}\text{CH}_2\text{D}_2$ deviations from equilibrium when endmembers are similar in $\delta^{13}\text{C}$ values but disparate in
377 δD values. Multiple two-component mixing scenarios can satisfy mixing relationships in the isotopologue
378 space. For example, in **Figure 5** we show a two-component mixing model between a gas equilibrated at 400°C
379 and a microbial gas with characteristic $\Delta^{12}\text{CH}_2\text{D}_2$ deficits. The high-T endmember $\delta^{13}\text{C}$ and δD values are taken
380 to be similar to the values observed at Lucky Strike for illustration. Approximately 20 to 25% of a microbial
381 gas mixed with high-temperature gas like that at the other vent sites can explain the methane isotopologue
382 data at Lost City (**Figure 5, panel a**). However, for the mixing loop to reach the compositions of the Lost City
383 samples, unusually high $\delta^{13}\text{C}$ values of between -35‰ and -20‰ must be ascribed to the microbial methane
384 component (**Fig. 5, panel b**). This is because the bulk isotopes and clumped isotopologue values, by design, do
385 not vary independently. Such high $\delta^{13}\text{C}$ values would be considered unreasonable for microbial methane in
386 most systems (Whiticar, 1999), but may be conceivable at Lost City, where biomarkers were observed with
387 extraordinarily high $\delta^{13}\text{C}$ values (Bradley et al. 2009). This mixing scenario, however, fails to match the data
388 trends where bulk isotope ratios are considered, including $\delta^{13}\text{C}$ vs. δD and $\Delta^{13}\text{CH}_3\text{D}$ vs. $\delta^{13}\text{C}$ (**Figure 5, panel b**
389 **and c respectively**). Conversely, when mixing is successful in panels comparing bulk isotopes and clumped
390 isotopes (**Fig. 5, panel b and d**), it fails at accounting for the data in mass-18 isotopologue space (**Figure 5, panel**
391 **a**). For this reason, we conclude that mixing with a microbial methane component is not the main source of the
392 anomalously high $\Delta^{12}\text{CH}_2\text{D}_2$ values at Lost City. An alternative mixing scenario involves two gases both at
393 isotopologue thermodynamic equilibrium at two disparate temperatures (**Figure 5**). A ~50:50 mixing of two
394 gases, one on the equilibrium curve at 400°C , and the other on the equilibrium curve at any temperature $<$
395 150°C , could fit the Lost City isotopologue and bulk isotope data as long as the $\delta^{13}\text{C}$ and δD of the endmembers
396 are restricted to a tight range of values. An example is shown in **Fig. 5**, with a gas taken at 100°C for illustration
397 (curve 2). The 100°C gas at Lost City would have to have $\delta^{13}\text{C}$ values $\geq -8\text{‰}$, and corresponding δD values of
398 -170‰ and lower. This is at the high- $\delta^{13}\text{C}$ and low- δD end of the empirically-defined abiotic field in **Figure 2**
399 (Etiope and Sherwood Lollar, 2013; Whiticar, 1999). The high $\delta^{13}\text{C}$ would be consistent with the near-
400 quantitative reduction of magmatic CO_2 (Horita and Berndt, 1999). The required δD value of -170‰ would
401 indicate a methane-water D/H equilibrium established at low temperature compared to Rainbow, Lucky Strike,

402 or Von Damm (Horibe and Craig, 1995), consistent with the bond-ordering inferences. However, again, this
403 type of mixing relationship fails to account for the details of the data trend in panel b of Figure 5. Where the
404 mixing proportions needed in the isotopologue plot (Fig. 5, panel a) are roughly 50-50, they are about 80-20 in
405 the bulk isotope space (Fig. 5 panel c), causing a mismatch in Figure 5, panel b.

406 Mixing involving a microbial endmember seems to be ruled out, and mixing between gases equilibrated at
407 high and low temperatures yields imperfect fits to the methane isotopologue and bulk isotope data taken
408 together. If mixing cannot satisfy the data in Fig. 5, we speculate that this is because $\Delta^{12}\text{CH}_2\text{D}_2$ was altered by
409 re-ordering at the temperature of the ambient fluids in the vent system at shallow depths. The near-perfect
410 match between $\Delta^{12}\text{CH}_2\text{D}_2$ -based temperatures and fluid temperatures (Fig. 4) argues in favor of $\Delta^{12}\text{CH}_2\text{D}_2$ re-
411 ordering. This conclusion is independent of the initial isotopologue composition of the abiotic methane, be it
412 on the equilibrium curve or below the equilibrium curve, as observed with the limited experimental evidence
413 (Young et al., 2017; see discussion above). We also suggest that the evidence for re-equilibration at Lost City
414 (Fig. 4) allows re-equilibration to have occurred at high-temperatures sites like Rainbow (see section 5.1). The
415 mechanism of re-equilibration remains unclear. In the laboratory, methane isotopologues reorder only in the
416 presence of a metal catalyst or alumina (Eldridge et al., 2019; Stolper et al., 2014; Wang et al., 2019; Young et
417 al., 2017) when methane is in a gas phase, but no experiments exist for dissolved methane in water. At Lost City
418 (and in all other deep-sea hydrothermal sites), methane is dissolved in water. Since $\Delta^{12}\text{CH}_2\text{D}_2$ is evidently re-
419 ordered specifically at the exit temperature of the host fluids, the re-equilibration must have occurred in the
420 cooling fluid upon ascent, perhaps facilitated by the metals that occur in underlying serpentinites at Lost City
421 (Kelley et al. 2005, Fruh-Green et al., 2018) or in metal deposits in chimneys observed at other sites (Von
422 Damm, 1990). It is also possible that the re-equilibration of $\Delta^{12}\text{CH}_2\text{D}_2$ values is microbially mediated. The
423 Archeal community at Lost City includes anaerobic methane-oxidizing Archaea, ANME-1 (Brazelton et al.,
424 2010). Equilibration of $\Delta^{12}\text{CH}_2\text{D}_2$ values has been attributed to anaerobic oxidation of methane (AOM) at
425 several localities, notably in gases from the Baltic Sea and the Western Ontario Basin (Young et al., 2017; Giunta
426 et al. 2019; Ash et al., 2019). However, the evidence for equilibration by AOM has been circumstantial and yet
427 to be demonstrated conclusively in the laboratory, and would not account for the equilibrated $\Delta^{12}\text{CH}_2\text{D}_2$ data

428 at Rainbow, Von Damm and Lucky Strike, where temperatures are above 122 °C, often considered the upper
429 limit for life (Takai et al. 2008).

430 In all cases, the data suggest that bond re-ordering is substantially slower for $\Delta^{13}\text{CH}_3\text{D}$, as if re-ordering was
431 inhibited when the isotopologue includes ^{13}C rather than ^{12}C . The mechanism allowing one
432 isotopologue, $^{12}\text{CH}_2\text{D}_2$, to be re-ordered to fluid temperature, while $^{13}\text{CH}_3\text{D}$ remains seemingly constant
433 deserves experimental attention. The observation that $\Delta^{12}\text{CH}_2\text{D}_2$ is prone to re-equilibration at lower
434 temperatures while $\Delta^{13}\text{CH}_3\text{D}$ is not suggests that the abundances of $^{13}\text{CH}_3\text{D}$ may represent a geochemical
435 indicator that preserves information about temperatures associated with methane formation, even when the
436 methane is transported at low temperatures prior to venting. The latter point is consistent with an earlier
437 suggestion based on $\Delta^{13}\text{CH}_3\text{D}$ measurements alone (Wang et al. 2018), but it is verified and underscored by the
438 contrasting behaviors of the two mass-18 isotopologues of methane at the vents studied here. The value of the
439 $\Delta^{12}\text{CH}_2\text{D}_2$ values may lie with their sensitivity to subsequent environmental conditions.

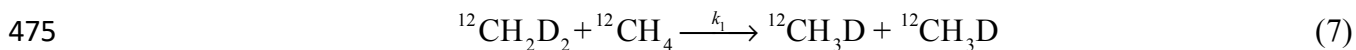
440 A caveat to the basic picture described above arises from the observation of a $\sim 1.5\text{‰}$ $\Delta^{13}\text{CH}_3\text{D}$ variability
441 at Lost City, when the *Beehive Marker C* and *Marker 2* vents are compared. To explain this in the context of just
442 one high-temperature source of methane at Lost City (Lang et al., 2012), one must invoke partial re-ordering
443 of $\Delta^{13}\text{CH}_3\text{D}$. The implication is that the cooling that resets $\Delta^{12}\text{CH}_2\text{D}_2$ values also partially re-equilibrates
444 $\Delta^{13}\text{CH}_3\text{D}$ values. High-temperature methane formed at ~ 330 °C would exhibit $\Delta^{13}\text{CH}_3\text{D}$ values of $\sim 1.5\text{‰}$. At 85
445 °C, thermodynamic equilibrium drives $\Delta^{13}\text{CH}_3\text{D}$ to $\sim 4\text{‰}$. *Beehive, Marker C*, and *Marker 2* are vented at 96°C,
446 81 °C and 64 °C, respectively, where the expectation of a $\Delta^{13}\text{CH}_3\text{D}$ trending towards $\sim 4\text{‰}$ because of partial
447 re-equilibration is valid. One may speculate that cooling allowed partial reordering of $\Delta^{13}\text{CH}_3\text{D}$ to $1.9\pm 0.2\text{‰}$ at
448 *Beehive* and $2.3\pm 0.2\text{‰}$ at *Marker C*. The ANME-1 identified at *Marker 2* (Brazelton et al., 2006) may be poorly
449 suited to process methane in Lost City (Lang et al. 2018) but if any biological mediation of methane occurred,
450 it might have affected $\Delta^{13}\text{CH}_3\text{D}$ at *Marker 2*, raising the values to $3.0\pm 0.2\text{‰}$ there. The advantage of the
451 hypothesis for partial $\Delta^{13}\text{CH}_3\text{D}$ re-equilibration at Lost City is that it explains why gases with higher $\Delta^{13}\text{CH}_3\text{D}$
452 are only observed in the coldest vents. It also removes the need for multiple methane pools, which is

453 inconsistent with the broadly constant CH₄/⁴He ratio observed in the vents of Lost City (Proskurowski et al.
454 2008, Lang et al. 2012).

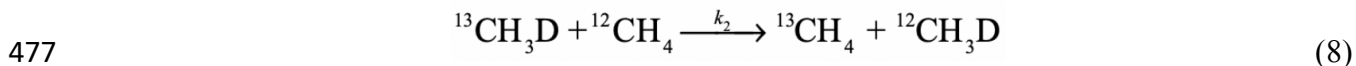
455 5.3 The relative vulnerability of ¹²CH₂D₂ to re-ordering

456 A process allowing $\Delta^{12}\text{CH}_2\text{D}_2$ to be equilibrated at fluid temperature during conductive cooling, while
457 $\Delta^{13}\text{CH}_3\text{D}$ remains broadly constant, appears to account for natural data. This process calls for differences in re-
458 equilibration rates. Here we explore this possibility with a simple kinetic model for exchange. Sophisticated
459 models, where re-equilibration is driven by D/H exchange between methane and water, could be envisioned.
460 In this context, water would be a reactive intermediate for re-ordering of methane isotopologues. At Lost City,
461 this approach would be consistent with the overall lower D/H ratio for vented methane compared to other
462 sites, suggesting some (but rather limited) D/H exchange occurred between methane and water during fluid
463 cooling (Proskurowski et al., 2006, Reeves et al., 2012). As a first approximation, we explore the specific case
464 of exchange of H and D between methane molecules. Our result based on molecular symmetry turns out to be
465 the same if we use water as the exchange partner. In either case, the stretched bond permitting the fleeing of
466 a protium or deuterium from a methane molecule is the reaction coordinate. We can describe the transition
467 state formed by this stretching symbolically, in the case of CH₄, as CH₃-H. The relative magnitudes of rate
468 constants for exchange reactions among isotopologues are dominated by differences in symmetry numbers, as
469 can be deduced from the analysis by Haghnegahdar et al. (2017). Indeed, both kinetic rate constants and
470 equilibrium constants for the mass-18 isotopologues are controlled to first order by differences in symmetry
471 numbers of the molecules. For example, the high-temperature limits for the equilibrium constants shown in
472 Equations (5) and (6) are 1 and 3/8, respectively, both corresponding to the relevant ratios of reactant and
473 product symmetry numbers.

474 Consider the reactions



476 and



478 One may apply transition state theory and write the reaction in terms of the transition state for one molecule
 479 that will control the rate of the reaction, treating the deuterated reactant as rate limiting in a matrix of
 480 exchangeable CH₄ gas (or, as it turns out, H₂O). While the full equation that includes vibrational and rotational
 481 partition functions is necessary for capturing isotope ratios in detail at the per mil level of precision, the rate
 482 constant ratio can be well approximated for our purposes using the ratio of symmetry numbers for the
 483 transition states and the reactants where σ_i are the symmetry numbers. For this purpose, we use the known
 484 symmetry numbers for the reactants: $\sigma_{^{12}\text{CH}_4} = 12$, $\sigma_{^{13}\text{CH}_3\text{D}} = 3$, and $\sigma_{^{12}\text{CH}_2\text{D}_2} = 2$ and recall that the rotational
 485 partition functions are proportional to the inverse of the symmetry numbers. We estimate the likely symmetry
 486 numbers for the transition states CH₂D-D* and ¹³CH₃-D* based on previous work (Haghnegahdar et al., 2017).
 487 Stretching of the ¹²CH₂D₂ molecule to donate a D to ¹²CH₄ should result in a highly asymmetric transition state
 488 with $\sigma_{\text{CH}_2\text{D-D}^*} = 1$. The transition state for ¹³CH₃D involves stretching the one ¹³C-D bond, forming ¹³CH₃-D*, and
 489 preserving the symmetry of ¹³CH₃D, yielding $\sigma_{\text{CH}_3\text{-D}^*} = 3$. We therefore have for the rate constant ratio

$$490 \quad \frac{k_{\text{CH}_2\text{D}_2}}{k_{^{13}\text{CH}_3\text{D}}} \sim \frac{\sigma_{\text{CH}_2\text{D}_2} \sigma_{\text{CH}_4}}{\sigma_{\text{CH}_2\text{D-D}^*} \sigma_{^{13}\text{CH}_3\text{D}}} \frac{\sigma_{^{13}\text{CH}_3\text{-D}^*}}{\sigma_{^{13}\text{CH}_3\text{D}} \sigma_{\text{CH}_4}} = \frac{2 \times 12}{1} \frac{3}{3 \times 12} = 2 \quad (9)$$

491 This result shows that the reaction involving the re-equilibration of ¹²CH₂D₂ can be expected to have a rate
 492 constant that is twice that for ¹³CH₃D. In practice, this means that during conductive cooling of a fluid, simple
 493 symmetry effects will lead $\Delta^{12}\text{CH}_2\text{D}_2$ to equilibrate twice as fast to environmental temperature than $\Delta^{13}\text{CH}_3\text{D}$.
 494 Because the symmetry number of the exchange partner (¹²CH₄ as written) cancels in Equation (9), substituting
 495 H₂O for ¹²CH₄, where $\sigma_{\text{H}_2\text{O}} = 2$, gives the same ratio of rate constants. We note, however, that the geometries
 496 associated with CH₄-H₂O exchange are highly uncertain (e.g., Mourik and Duijneveldt 1995; Cappelletti et al.
 497 2015; Richardson et al. 2016).

498 In order to apply these rate constants to the exchange process, we make use of rate equations for
 499 kinetic isotope exchange expressed in terms of fractional approaches to equilibrium (Criss et al., 1987) for the
 500 reactions in Equations (7) and (8), respectively:

$$501 \quad \frac{[^{12}\text{CH}_2\text{D}_2]_t - [^{12}\text{CH}_2\text{D}_2]_{\text{EQ}}}{[^{12}\text{CH}_2\text{D}_2]_0 - [^{12}\text{CH}_2\text{D}_2]_{\text{EQ}}} = e^{-k_{\text{CH}_2\text{D}_2} t} \quad (10)$$

502 and

$$\frac{[^{13}\text{CH}_3\text{D}]_t - [^{13}\text{CH}_3\text{D}]_{\text{EQ}}}{[^{13}\text{CH}_3\text{D}]_0 - [^{13}\text{CH}_3\text{D}]_{\text{EQ}}} = e^{-k_{^{13}\text{CH}_3\text{D}} t} \quad (11)$$

503

504 where subscript t refers to time, subscript o refers to initial concentrations, and subscript EQ refers to the
 505 equilibrium concentrations for the isotopologues.

506 The re-equilibration mechanism with various rate constant ratios is plotted on figure 2, alongside the
 507 data. We explore whether the trajectory of a gas equilibrated at high temperatures undergoing cooling matches
 508 the Lost City observation. We take the low-temperature endpoint to be constrained by the measured
 509 temperature in the relevant Lost City vents, at 65 °C. Although the rate constant ratio of 2 resulting from
 510 Equation (9) yields a trajectory in the right direction, it does not fully account for the data. We find that a rate
 511 constant ratio $k_{\text{CH}_2\text{D}_2}/k_{^{13}\text{CH}_3\text{D}}$ of ~ 5 is required to explain the data (Fig. 2). Again, our data highlight the need for
 512 experimental work to explore whether these re-equilibration patterns are to be expected on a physicochemical
 513 basis. The simple theoretical framework explored here may offer a first order guide to how methane
 514 isotopologues behave during fluid cooling in natural settings.

515 Conclusion

516 We report $\Delta^{13}\text{CH}_3\text{D}$ and $\Delta^{12}\text{CH}_2\text{D}_2$ data in methane samples from deep-sea hydrothermal systems. We show
 517 that in the hottest fluids at the Rainbow site, concordant temperatures are recorded by the two mass-18
 518 isotopologues. Thus, methane is in internal thermodynamic equilibrium. In the other sites, we observe variable
 519 $\Delta^{12}\text{CH}_2\text{D}_2$ at nearly constant $\Delta^{13}\text{CH}_3\text{D}$. The data exclude mixing with microbial gas; mixing produces imperfect
 520 fits to the bulk isotope ratios and isotopologue abundances. The variable $\Delta^{12}\text{CH}_2\text{D}_2$ values correlate
 521 surprisingly well with fluid temperatures and thus we suggest they record rapid $^{12}\text{CH}_2\text{D}_2$ re-equilibration in
 522 cooling hydrothermal fluids upon ascent. None of the isotopologue signatures resemble those obtained from
 523 experimental investigations of abiotic CH_4 synthesis in the laboratory, nor do they resemble the isotopologue
 524 signatures of abiotic methane formation in natural settings to date. The mechanism of re-equilibration in the
 525 case of these deep-sea hydrothermal fluids but not in the case of Kidd Creek cold fluids deserves experimental
 526 investigation. The discovery of resetting of $\Delta^{12}\text{CH}_2\text{D}_2$ values during transport affords the opportunity to use
 527 these values in concert with $\Delta^{13}\text{CH}_3\text{D}$ values to obtain a more complete picture of the thermal evolution of

528 methane gases. This is because $\Delta^{12}\text{CH}_2\text{D}_2$ appears to be completely reset to fluid temperatures in a wide
 529 temperature range, between 360 and 65°C. In contrast, $\Delta^{13}\text{CH}_3\text{D}$ shows limited evidence for re-ordering. We
 530 suggest that to first order, equilibration of $\Delta^{12}\text{CH}_2\text{D}_2$ should be faster than that for $\Delta^{13}\text{CH}_3\text{D}$ by a factor of ~ 2 ,
 531 but further investigation on relative rates of reaction is warranted. Because the apparent $\Delta^{13}\text{CH}_3\text{D}$ -based
 532 temperatures greatly exceed those amenable to microbial life in all sites, and because the isotopologue data
 533 rule out mixing with microbial gases, our data indicate that methane formation at all of the sites, including Lost
 534 City, is probably dominantly abiotic.

535

536 Acknowledgements

537 We acknowledge support from the Deep Carbon Observatory Deep Energy grants G-2018-11346 and G-
 538 2017-9815 to EdY. We acknowledge Susan Lang for leading the 2018 Lost City cruise and for providing the
 539 temperature data funded by NSF-OCE-1536702 and a DCO-Deep Life sub-awards. We thank Tamara
 540 Baumberger for shipboard assistance with processing the gas samples. We thank Shuhei Ono and David Wang
 541 for sharing samples. We thank Orit Sivan and four anonymous reviewers for comments that improved the
 542 manuscript.

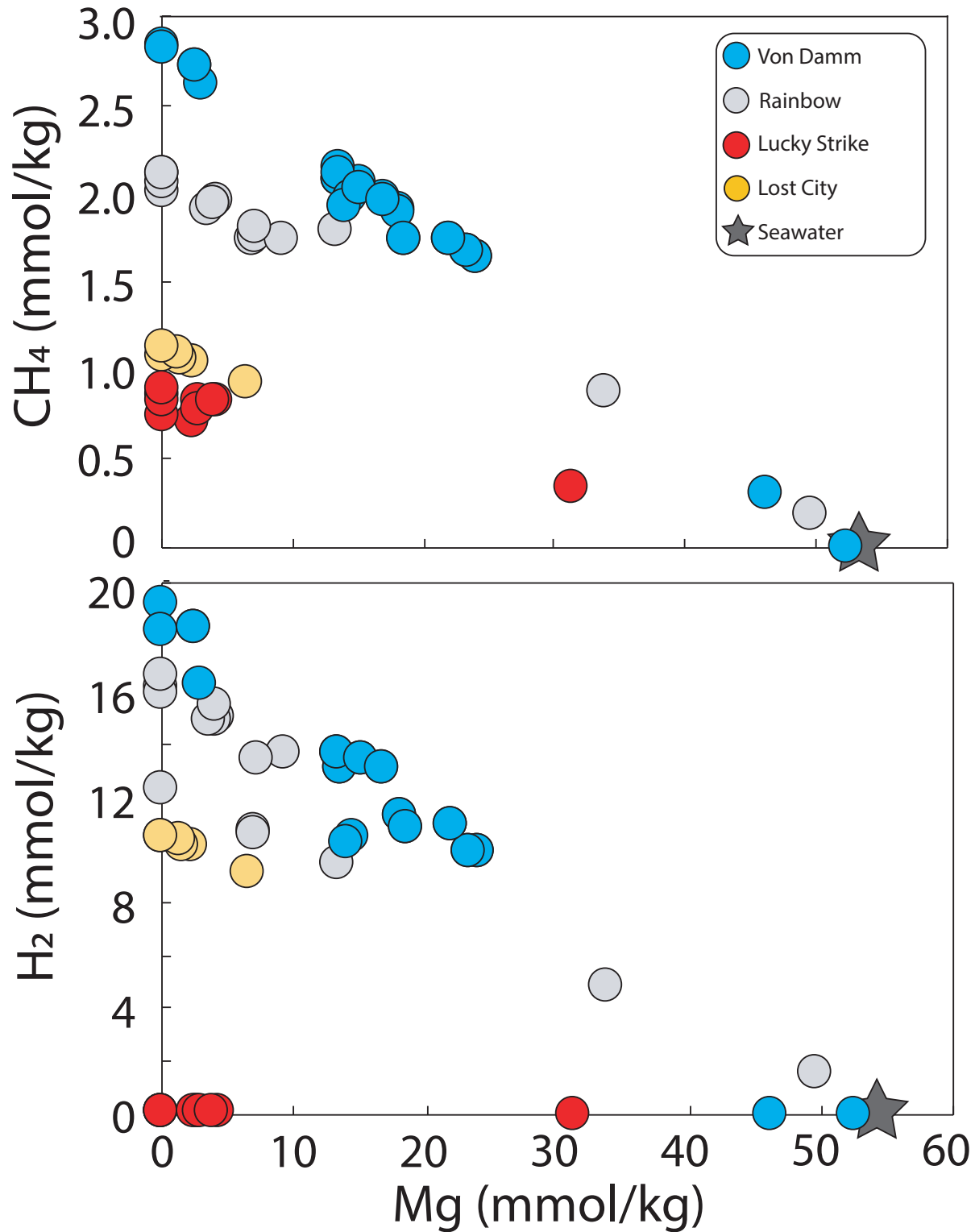
543

544 Captions

Site	vent	sample ID	CH ₄ quantity (μmol)	endmember temperature (C)	$\delta^{13}\text{C}$ PDB	δD SMOW	$\Delta^{13}\text{CH}_3\text{D}$	1 se	$\Delta^{12}\text{CH}_2\text{D}_2$	1 se
Rainbow	guillaume	J2-352-IGT4	38.8	361	-16.71	-98.06	1.6	0.3	2.7	0.8
	CMSP_and_P	J2-354-IGT3	51.3	365	-17.03	-98.49	1.2	0.2	3.5	0.8
	Auberge	J2-352-IGT3	46.8	370	-16.96	-98.07	1.3	0.2	1.7	1.0
Von Damm	Ravelin	J2-617-IGT6	45.0	226	-15.72	-107.26	1.4	0.3	4.4	1.0
	Summit	J2-612-IGT2	40.0	228	-16.50	-113.08	1.7	0.4	4.5	1.8
Lost City	Beehive	J2-361-IGT5	62.5	96	-10.80	-127.11	1.9	0.2	10.7	0.9
	Beehive	H06_GT_15/16	85.0	96	-10.84	-127.84	1.9	0.2	11.6	0.5
	marker 2	j1107 GT	75.0	64	-9.62	-143.31	3.0	0.2	14.5	1.0
	marker 2	J1111 titan	120.0	64	-7.58	-141.48	2.3	0.2	13.8	0.6
	marker c	j1110 titan	90.0	81	-10.61	-129.70	2.3	0.2	11.3	0.8
	marker c	j1110 GT	50.0	81	-10.97	-130.19	2.0	0.2	12.3	1.4
Lucky Strike	Isabel	J2-357-IGT5	47.5	292	-12.03	-100.72	1.0	0.2	2.9	0.7

545

546 Table 1: Methane isotope data for hydrothermal fluids. bulk $^{13}\text{C}/^{12}\text{C}$ and D/H are reported alongside $\Delta^{13}\text{CH}_3\text{D}$
547 and $\Delta^{12}\text{CH}_2\text{D}_2$.
548 Analytical uncertainties are below 0.1‰ (95% confidence intervals) for $\delta^{13}\text{C}$ and δD . Propagated uncertainties
549 are listed for $\Delta^{13}\text{CH}_3\text{D}$ and $\Delta^{12}\text{CH}_2\text{D}_2$ in 1σ . They are variable from a sample to another, depending mostly on
550 counting statistics. Hence the magnitude of the uncertainties for both $\Delta^{13}\text{CH}_3\text{D}$ and $\Delta^{12}\text{CH}_2\text{D}_2$ are a simple
551 function of the processed CH_4 quantity (in μmol). Temperature data are extracted from the literature
552 (McDermott et al. 2015, Reeves et al. 2014, but see also Pester et al. 2012, Charlou et al. 2010, Seyfried et al.,
553 2011).
554
555

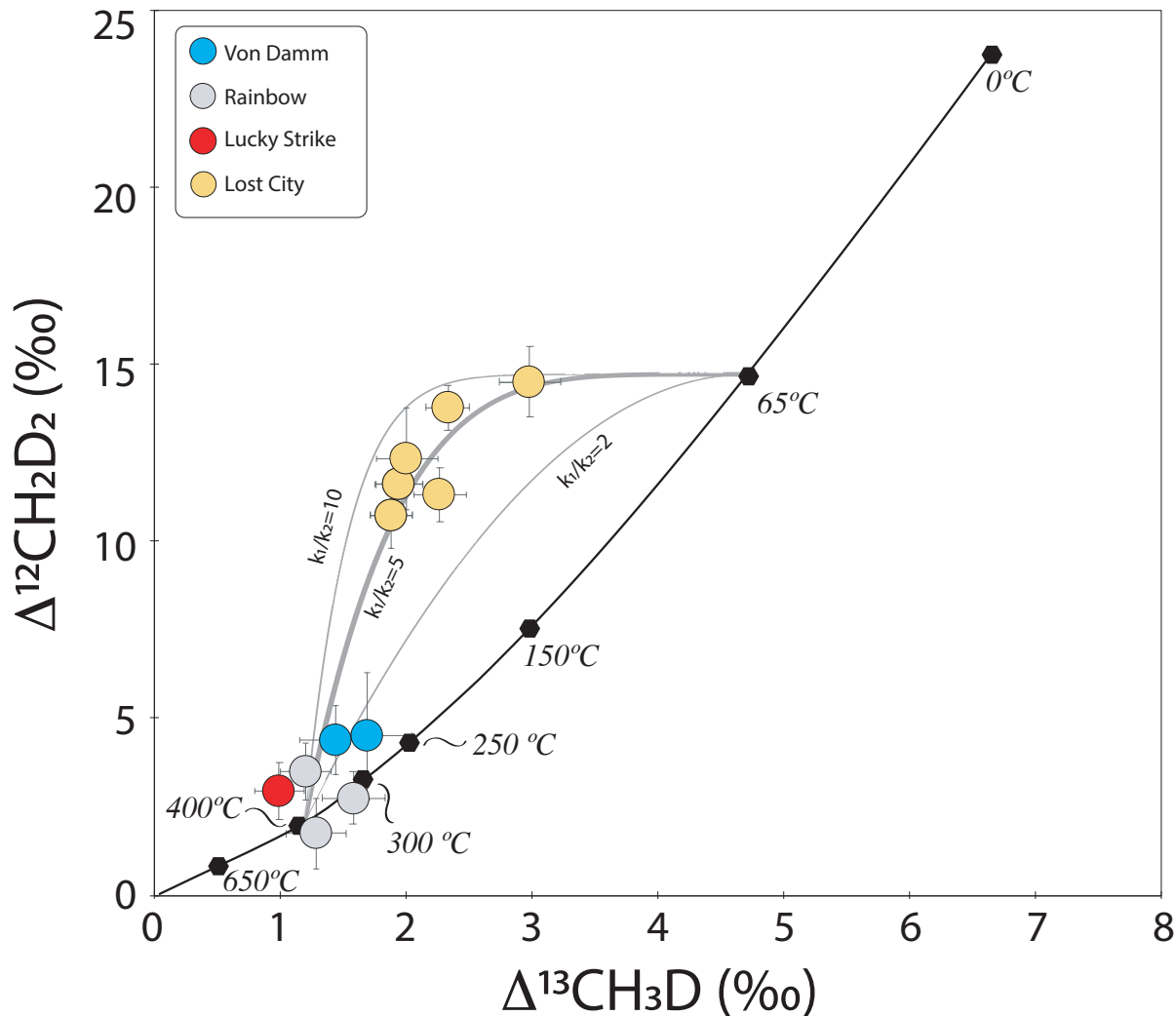


556

557 Figure 1: Dissolved methane and hydrogen concentrations in hydrothermal fluids from the five locations

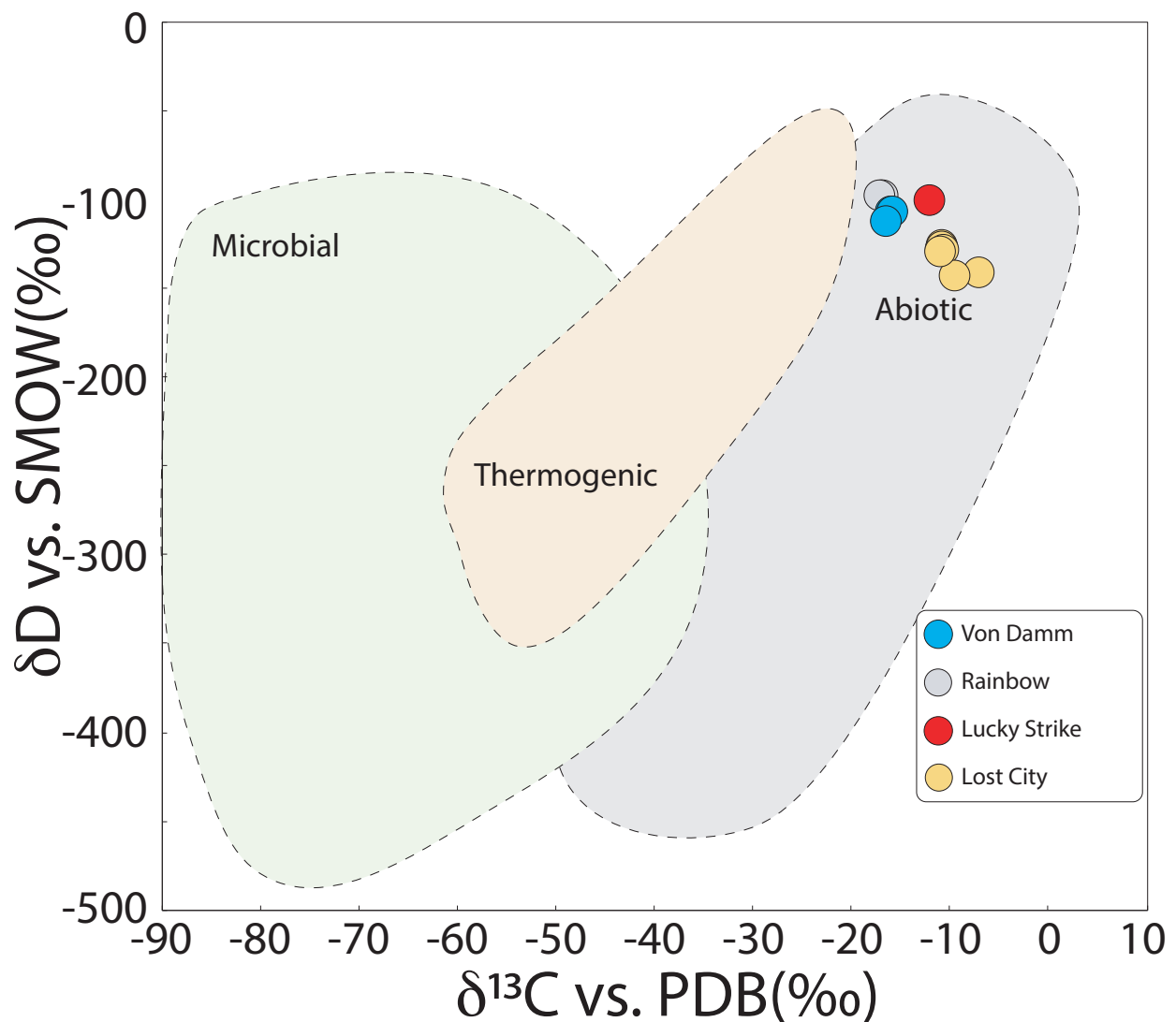
558 studied here plotted against Mg concentrations. Data are from Reeves et al. (2014) and McDermott et al. (2015).

559 With the exception of a sample from Vom Damm, *Ravelin*, all the samples studied here have Mg concentrations
 560 5 mmol/kg (Data in Reeves et al., 2014, McDermott et al., 2015, and this study). *Ravelin*, however, shows a
 561 concentration of ~16 mmol/kg, together with a lower temperature than the local fluid endmember (Reeves et
 562 al., 2014). This one gas can be accounted for by seawater infiltration, abruptly lowering temperature venting.
 563



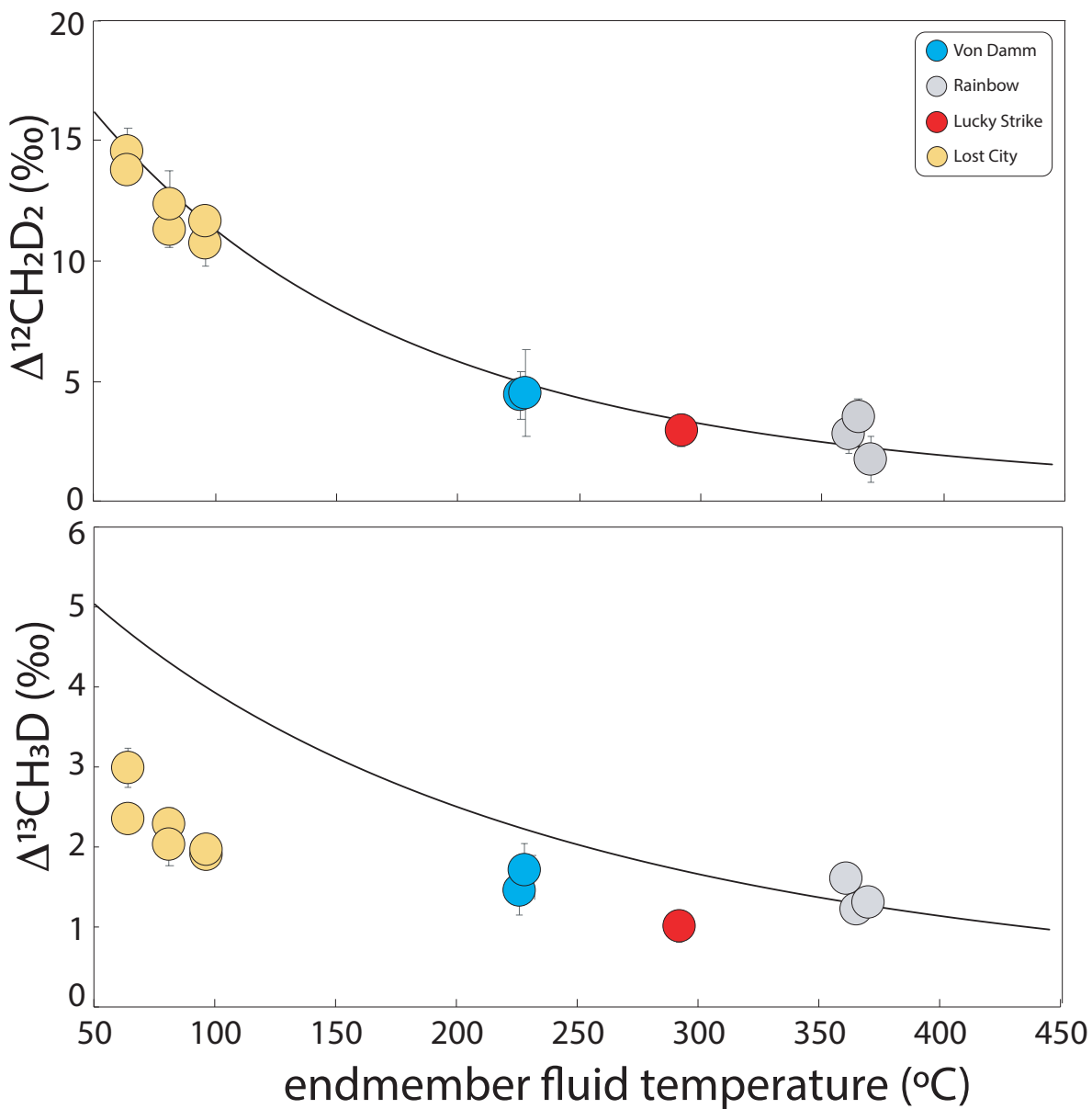
564
 565 Figure 2: Plot of $\Delta^{12}\text{CH}_2\text{D}_2$ vs. $\Delta^{13}\text{CH}_3\text{D}$ for methane samples from the hydrothermal vent systems that are part
 566 of this study. The curve representing thermodynamic equilibrium is shown for reference, along with
 567 corresponding temperatures. While Rainbow shows equilibrium signatures, Von Damm and Lucky Strike
 568 display marginally high $\Delta^{12}\text{CH}_2\text{D}_2$. The Lost City samples display considerable $\Delta^{12}\text{CH}_2\text{D}_2$ enrichments at a given

569 $\Delta^{13}\text{CH}_3\text{D}$ value. Data and uncertainties are from Table 1. Re-equilibration trajectories are plotted using the
570 equations in section 5.3. Three scenarios are shown with three different ratios for the exchange rate constants
571 for $\Delta^{12}\text{CH}_2\text{D}_2$ and $\Delta^{13}\text{CH}_3\text{D}$ (see text). Note that the endmember low temperature is picked at 65 °C for
572 illustration. This corresponds to the approximate temperature of the fluid from *marker 2*, the coldest vent
573 studied here. For the Beehive vent, a temperature of 96 °C would be required for the low-temperature
574 endmember. Although not shown here for the sake of clarity, such an endmember temperature fits the Beehive
575 data if $k_1 \sim 5 \times k_2$.

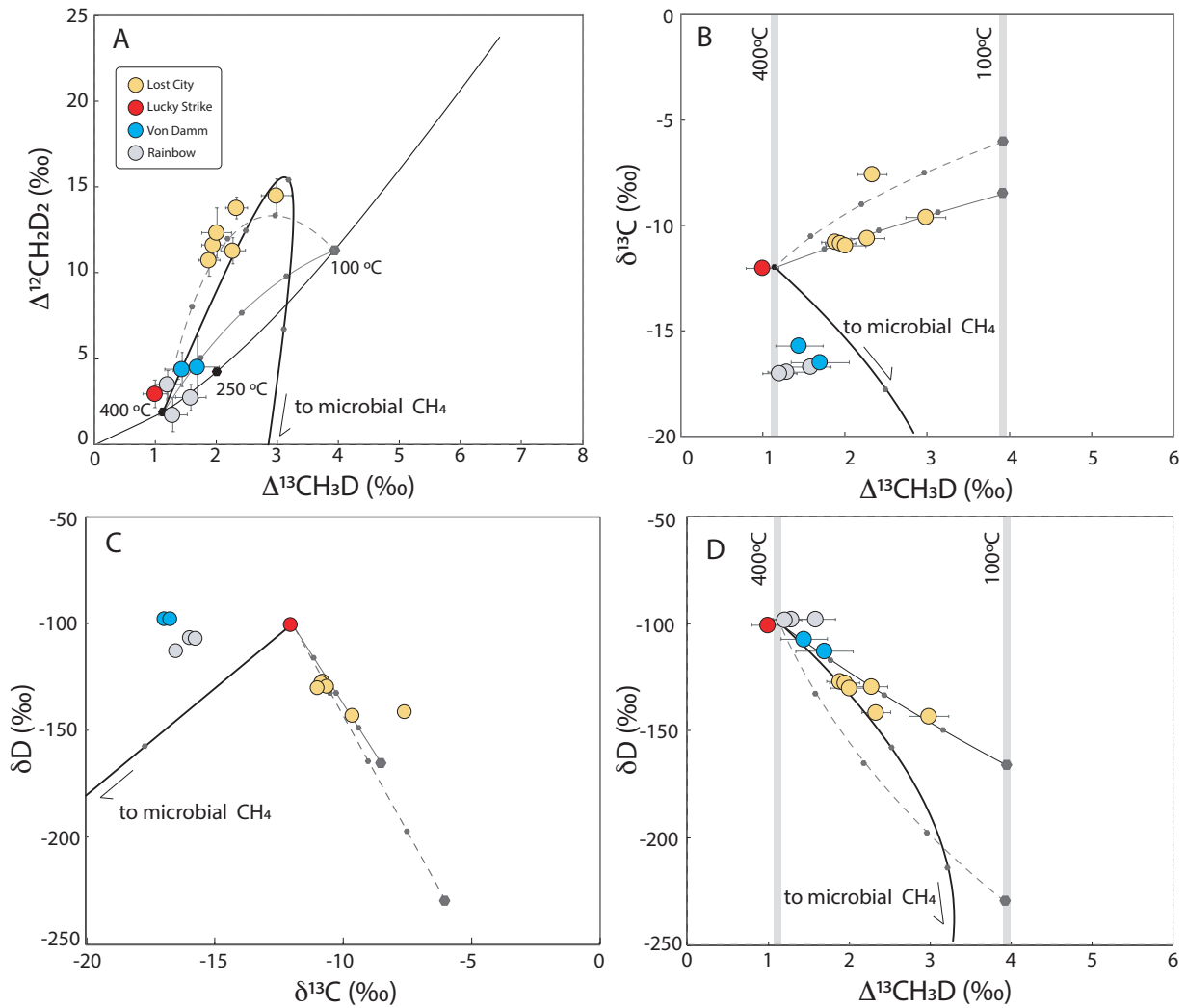


576
577 Figure 3: δD and $\delta^{13}\text{C}$ values of methane samples in the “Schoell” plot (Schoell, 1988). Fields are suggested by
578 those from Etiope and Sherwood Lollar (2013). As suggested in previous work (Wang et al., 2018,

579 Proskurowski et al. 2008, Charlou et al., 2010, McDermott et al., 2015), methane in deep-sea hydrothermal field
580 plots defines the extremity of the abiotic field. Data and uncertainties are from Table 1.



581
582 Figure 4: Plot showing the relationship between the two mass-18 isotopologues of methane samples from the
583 hydrothermal systems and the endmember temperatures of the fluid containing the methane. Note the
584 correlation with fluid temperatures exhibited by $\Delta^{12}\text{CH}_2\text{D}_2$ but not $\Delta^{13}\text{CH}_3\text{D}$ values. Data and uncertainties are
585 from Table 1.



586

587 Figure 5. Mixing scenarios for methane from Lost City, examined in 4 different CH₄ isotopic spaces. Dots
 588 represent 25% increases in mixing increments. The bold curve is mixing between high-temperature gas and a
 589 microbial gas (see text) and shown by the bold plain curve. The dashed curve represents a two-component
 590 mixing between two equilibrated gases, at distinct temperatures, with endmember composition fit to account
 591 for the data in panel A and C. The plain thin curve is a two-component mixing between two equilibrated gases,
 592 at distinct temperatures, with endmember composition fit to account for the data in panel B, C and D. The panel
 593 A shows the two endmember possibilities that could fit the clumped isotopologue data, where $\Delta^{12}\text{CH}_2\text{D}_2$ is
 594 plotted vs. $\Delta^{13}\text{CH}_3\text{D}$. Panel B, C and D shows the various bulk-isotope trajectories of the model that is seemingly
 595 successful in panel A. We find no mixing scenario that accounts for all of the trends defined by the data.
 596

- 598 Allen, D.E., Seyfried Jr, W., 2004. Serpentinization and heat generation: constraints from Lost City
599 and Rainbow hydrothermal systems. *Geochimica et Cosmochimica Acta* 68, 1347-1354.
- 600 Ash, J.L., Egger, M., Treude, T., Kohl, I., Cragg, B., Parkes, R.J., Slomp, C.P., Sherwood Lollar, B.,
601 Young, E.D., 2019. Exchange catalysis during anaerobic methanotrophy revealed by $^{12}\text{CH}_2\text{D}_2$ and
602 $^{13}\text{CH}_3\text{D}$ in methane. *geochemical Perspect. Lett.* 10, 26–30.
- 603 Berndt, M.E., Allen, D.E., Seyfried, W.E., 1996. Reduction of CO_2 during serpentinization of olivine
604 at 300 °C and 500 bar. *Geology* 24, 351-354.
- 605 Bradley, A.S., Summons, R.E., 2010. Multiple origins of methane at the lost City hydrothermal
606 field. *Earth and Planetary Science Letters* 297, 34-41.
- 607 Brazelton, W.J., Schrenk, M.O., Kelley, D.S., Baross, J.A., 2006. Methane-and sulfur-metabolizing
608 microbial communities dominate the Lost City hydrothermal field ecosystem. *Appl. Environ.*
609 *Microbiol.* 72, 6257-6270.
- 610 Cappelletti, D., Bartocci, A., Frati, F., Roncaratti, L. F., Belpassi, L., Tarantelli, F., ... & Pirani, F.,
611 2015. $\text{H}_2\text{O}-\text{CH}_4$ and $\text{H}_2\text{S}-\text{CH}_4$ complexes: a direct comparison through molecular beam
612 experiments and ab initio calculations. *Physical Chemistry Chemical Physics*, 17(45), 30613-
613 30623.
- 614 Cao, X., Bao, H., Peng, Y., 2019. A kinetic model for isotopologue signatures of methane
615 generated by biotic and abiotic CO_2 methanation. *Geochimica et Cosmochimica Acta* 249, 59-75.
- 616 Charlou, J., Donval, J., Douville, E., Jean-Baptiste, P., Radford-Knoery, J., Fouquet, Y., Dapoigny,
617 A., Stievenard, M., 2000. Compared geochemical signatures and the evolution of Menez Gwen
618 (37°50' N) and Lucky Strike (37°17' N) hydrothermal fluids, south of the Azores Triple Junction on
619 the Mid-Atlantic Ridge. *Chemical geology* 171, 49-75.
- 620 Charlou, J.L., Donval, J.P., Fouquet, Y., Jean-Baptiste, P., Holm, N., 2002. Geochemistry of high H_2
621 and CH_4 vent fluids issuing from ultramafic rocks at the Rainbow hydrothermal field (36°14'N,
622 MAR). *Chemical Geology* 191, 345-359.
- 623 Charlou, J.L., Donval, J.P., Konn, C., OndréAs, H., Fouquet, Y., Jean-Baptiste, P., Fourré, E., 2010.
624 High production and fluxes of H_2 and CH_4 and evidence of abiotic hydrocarbon synthesis by
625 serpentinization in ultramafic-hosted hydrothermal systems on the Mid-Atlantic Ridge. *Diversity*
626 *of hydrothermal systems on slow spreading ocean ridges* 188, 265-296.
- 627 Connelly, D.P., Copley, J.T., Murton, B.J., Stansfield, K., Tyler, P.A., German, C.R., Van Dover, C.L.,
628 Amon, D., Furlong, M., Grindlay, N., 2012. Hydrothermal vent fields and chemosynthetic biota on
629 the world's deepest seafloor spreading centre. *Nature Communications* 3, 1-9.
- 630 Criss, R., Gregory, R., Taylor Jr, H., 1987. Kinetic theory of oxygen isotopic exchange between
631 minerals and water. *Geochimica et Cosmochimica Acta* 51, 1099-1108.
- 632 Eldridge, D.L., Korol, R., Lloyd, M.K., Turner, A.C., Webb, M.A., Miller III, T.F., Stolper, D.A., 2019.
633 Comparison of Experimental vs Theoretical Abundances of $^{13}\text{CH}_3\text{D}$ and $^{12}\text{CH}_2\text{D}_2$ for Isotopically
634 Equilibrated Systems from 1 to 500° C. *ACS Earth and Space Chemistry*.
- 635 Etiope, G., Ionescu, A., 2015. Low-temperature catalytic CO_2 hydrogenation with geological
636 quantities of ruthenium: a possible abiotic CH_4 source in chromitite-rich serpentinized rocks.
637 *Geofluids* 15, 438-452.
- 638 Etiope, G., Sherwood Lollar, B., 2013. Abiotic methane on Earth. *Reviews of Geophysics* 51, 276-
639 299.

640 Foustoukos, D.I., Mysen, B.O., 2013. H/D methane isotopologues dissolved in magmatic fluids:
641 Stable hydrogen isotope fractionations in the Earth's interior. *American Mineralogist* 98, 946-
642 954.

643 Foustoukos, D.I., Savov, I.P., Janecky, D.R., 2008. Chemical and isotopic constraints on water/rock
644 interactions at the Lost City hydrothermal field, 30°N Mid-Atlantic Ridge. *Geochimica et*
645 *Cosmochimica Acta* 72, 5457-5474.

646 Foustoukos, D.I., Seyfried, W.E., Jr., 2004. Hydrocarbons in Hydrothermal Vent Fluids: The Role
647 of Chromium-Bearing Catalysts. *Science* 304, 1002-1005.

648 Früh-Green, G.L., Orcutt, B.N., Rouméjon, S., Lilley, M.D., Morono, Y., Cotterill, C., Green, S.,
649 Escartin, J., John, B.E., McCaig, A.M., 2018. Magmatism, serpentinization and life: Insights
650 through drilling the Atlantis Massif (IODP Expedition 357). *Lithos* 323, 137-155.

651 Giunta, T., Young, E.D., Warr, O., Kohl, I., Ash, J.L., Martini, A., Mundle, S.O., Rumble, D., Pérez-
652 Rodríguez, I., Wasley, M., 2019. Methane sources and sinks in continental sedimentary systems:
653 New insights from paired clumped isotopologues $^{13}\text{CH}_3\text{D}$ and $^{12}\text{CH}_2\text{D}_2$. *Geochimica et*
654 *Cosmochimica Acta* 245, 327-351.

655 Grozeva, N.G., Klein, F., Seewald, J.S., Sylva, S.P., 2020. Chemical and isotopic analyses of
656 hydrocarbon-bearing fluid inclusions in olivine-rich rocks. *Philosophical Transactions of the Royal*
657 *Society A* 378, 20180431.

658 Haghnegahdar, M.A., Schauble, E.A., Young, E.D., 2017. A model for $^{12}\text{CH}_2\text{D}_2$ and $^{13}\text{CH}_3\text{D}$ as
659 complementary tracers for the budget of atmospheric CH_4 . *Global Biogeochemical Cycles* 31,
660 1387-1407.

661 Holm, N.G., Charlou, J.L., 2001. Initial indications of abiogenic formation of hydrocarbons in the
662 Rainbow ultramafic hydrothermal system, Mid-Atlantic Ridge. *Earth and Planetary Science*
663 *Letters* 191, 1-8.

664 Horibe, Y., Craig, H., 1995. DH fractionation in the system methane-hydrogen-water. *Geochimica*
665 *et Cosmochimica Acta* 59, 5209-5217.

666 Horita, J., Berndt, M.E., 1999. Abiogenic methane formation and isotopic fractionation under
667 hydrothermal conditions. *Science* 285, 1055-1057.

668 Jones, L.C., Rosenbauer, R., Goldsmith, J.I., Oze, C., 2010. Carbonate control of H_2 and CH_4
669 production in serpentinization systems at elevated P-Ts. *Geophysical Research Letters* 37,
670 L14306.

671 Kelley, D.S., 1996. Methane-rich fluids in the oceanic crust. *Journal of Geophysical Research: Solid*
672 *Earth* 101, 2943-2962.

673 Kelley, D.S., Früh-Green, G.L., 1999. Abiogenic methane in deep-seated mid-ocean ridge
674 environments: Insights from stable isotope analyses. *Journal of Geophysical Research: Solid Earth*
675 104, 10439-10460.

676 Kelley, D.S., Karson, J.A., Blackman, D.K., Früh-Green, G.L., Butterfield, D.A., Lilley, M.D., Olson,
677 E.J., Schrenk, M.O., Roe, K.K., Lebon, G.T., 2001. An off-axis hydrothermal vent field near the Mid-
678 Atlantic Ridge at 30 N. *Nature* 412, 145.

679 Kelley, D.S., Karson, J.A., Früh-Green, G.L., Yoerger, D.R., Shank, T.M., Butterfield, D.A., Hayes,
680 J.M., Schrenk, M.O., Olson, E.J., Proskurowski, G., 2005. A serpentinite-hosted ecosystem: the
681 Lost City hydrothermal field. *Science* 307, 1428-1434.

682 Klein, F., Grozeva, N.G., Seewald, J.S., 2019. Abiogenic methane synthesis and serpentinization in
683 olivine-hosted fluid inclusions. *Proceedings of the National Academy of Sciences*, 201907871.

684 Konn, C., Charlou, J.-L., Donval, J.-P., Holm, N., Dehairs, F., Bouillon, S., 2009. Hydrocarbons and
685 oxidized organic compounds in hydrothermal fluids from Rainbow and Lost City ultramafic-
686 hosted vents. *Chemical Geology* 258, 299-314.

687 Lang, S.Q., Butterfield, D.A., Schulte, M., Kelley, D.S., Lilley, M.D., 2010. Elevated concentrations
688 of formate, acetate and dissolved organic carbon found at the Lost City hydrothermal field.
689 *Geochimica et Cosmochimica Acta* 74, 941-952.

690 Lang, S.Q., Früh-Green, G.L., Bernasconi, S.M., Lilley, M.D., Proskurowski, G., Méhay, S.,
691 Butterfield, D.A., 2012. Microbial utilization of abiogenic carbon and hydrogen in a serpentinite-
692 hosted system. *Geochimica et Cosmochimica Acta* 92, 82-99.

693 McCollom, T.M., 2013. Laboratory simulations of abiotic hydrocarbon formation in Earth's deep
694 subsurface. *Reviews in Mineralogy and Geochemistry* 75, 467-494.

695 McCollom, T.M., 2016. Abiotic methane formation during experimental serpentinization of
696 olivine. *Proc Natl Acad Sci U S A* 113, 13965-13970.

697 McCollom, T.M., Lollar, B.S., Lacrampe-Couloume, G., Seewald, J.S., 2010. The influence of carbon
698 source on abiotic organic synthesis and carbon isotope fractionation under hydrothermal
699 conditions. *Geochimica et Cosmochimica Acta* 74, 2717-2740.

700 McCollom, T.M., Seewald, J.S., 2001. A reassessment of the potential for reduction of dissolved
701 CO₂ to hydrocarbons during serpentinization of olivine. *Geochimica et Cosmochimica Acta* 65,
702 3769-3778.

703 McCollom, T.M., Seewald, J.S., 2007. Abiotic synthesis of organic compounds in deep-sea
704 hydrothermal environments. *Chemical Reviews* 107, 382-401.

705 McDermott, J.M., Seewald, J.S., German, C.R., Sylva, S.P., 2015. Pathways for abiotic organic
706 synthesis at submarine hydrothermal fields. *Proceedings of the National Academy of Sciences*.

707 Neubeck, A., Duc, N.T., Bastviken, D., Crill, P., Holm, N.G., 2011. Formation of H₂ and CH₄ by
708 weathering of olivine at temperatures between 30 and 70 C. *Geochemical Transactions* 12, 6.

709 Okland, I., Huang, S., Thorseth, I., Pedersen, R., 2014. Formation of H₂, CH₄ and N-species during
710 low-temperature experimental alteration of ultramafic rocks. *Chemical Geology* 387, 22-34.

711 Oze, C., Jones, L.C., Goldsmith, J.I., Rosenbauer, R.J., 2012. Differentiating biotic from abiotic
712 methane genesis in hydrothermally active planetary surfaces. *Proceedings of the National*
713 *Academy of Sciences* 109, 9750-9754.

714 Pester, N.J., Reeves, E.P., Rough, M.E., Ding, K., Seewald, J.S., Seyfried Jr, W.E., 2012. Subseafloor
715 phase equilibria in high-temperature hydrothermal fluids of the Lucky Strike Seamount (Mid-
716 Atlantic Ridge, 37° 17' N). *Geochimica et Cosmochimica Acta* 90, 303-322.

717 Proskurowski, G., Lilley, M.D., Seewald, J.S., Früh-Green, G.L., Olson, E.J., Lupton, J.E., Sylva, S.P.,
718 Kelley, D.S., 2008. Abiogenic hydrocarbon production at Lost City hydrothermal field. *Science*
719 319, 604-607.

720 Reeves, E.P., McDermott, J.M., Seewald, J.S., 2014. The origin of methanethiol in midocean ridge
721 hydrothermal fluids. *Proceedings of the National Academy of Sciences* 111, 5474-5479.

722 Reeves, E.P., Seewald, J.S., Sylva, S.P., 2012. Hydrogen isotope exchange between n-alkanes and
723 water under hydrothermal conditions. *Geochimica et Cosmochimica Acta* 77, 582-599.

724 Richardson, J. O., Pérez, C., Lobsiger, S., Reid, A. A., Temelso, B., Shields, G. C., ... & Althorpe, S.
725 C., 2016. Concerted hydrogen-bond breaking by quantum tunneling in the water hexamer
726 prism. *Science*, 351(6279), 1310-1313.

727 Röckmann, T., Popa, M.E., Krol, M., Hofmann, M., 2016. Statistical clumped isotope signatures.
728 Scientific reports 6, 31947.

729 Rouméjon, S., Früh-Green, G.L., Orcutt, B.N., Party, I.E.S., 2018. Alteration heterogeneities in
730 peridotites exhumed on the southern wall of the atlantis massif (IODP expedition 357). Journal
731 of Petrology 59, 1329-1358.

732 Schoell, M., 1988. Multiple origins of methane in the Earth. Chemical geology 71, 1-10.

733 Schrenk, M.O., Kelley, D.S., Bolton, S.A., Baross, J.A., 2004. Low archaeal diversity linked to
734 seafloor geochemical processes at the Lost City Hydrothermal Field, Mid-Atlantic Ridge.
735 Environmental Microbiology 6, 1086-1095.

736 Seewald, J.S., Zolotov, M.Y., McCollom, T.M., 2006. Experimental investigation of single carbon
737 compounds under hydrothermal conditions. Geochimica et Cosmochimica Acta 70, 446-460.

738 Seyfried Jr, W., Pester, N.J., Ding, K., Rough, M., 2011. Vent fluid chemistry of the Rainbow
739 hydrothermal system (36 N, MAR): Phase equilibria and in situ pH controls on seafloor
740 alteration processes. Geochimica et Cosmochimica Acta 75, 1574-1593.

741 Seyfried Jr, W., Pester, N.J., Tutolo, B.M., Ding, K., 2015. The Lost City hydrothermal system:
742 Constraints imposed by vent fluid chemistry and reaction path models on seafloor heat and
743 mass transfer processes. Geochimica et Cosmochimica Acta 163, 59-79.

744 Sherwood Lollar, B., Frape, S., Weise, S., Fritz, P., Macko, S., Welhan, J., 1993. Abiogenic
745 methanogenesis in crystalline rocks. Geochimica et Cosmochimica Acta 57, 5087-5097.

746 Sherwood Lollar, B., Lacrampe-Couloume, G., Slater, G., Ward, J., Moser, D., Gihring, T., Lin, L.-
747 H., Onstott, T., 2006. Unravelling abiogenic and biogenic sources of methane in the Earth's deep
748 subsurface. Chemical Geology 226, 328-339.

749 Sherwood Lollar, B., Westgate, T., Ward, J., Slater, G., Lacrampe-Couloume, G., 2002. Abiogenic
750 formation of alkanes in the Earth's crust as a minor source for global hydrocarbon reservoirs.
751 Nature 416, 522.

752 Stolper, D., Lawson, M., Davis, C., Ferreira, A., Neto, E.S., Ellis, G., Lewan, M., Martini, A.M., Tang,
753 Y., Schoell, M., 2014. Formation temperatures of thermogenic and biogenic methane. Science
754 344, 1500-1503.

755 Stolper, D., Martini, A., Clog, M., Douglas, P., Shusta, S., Valentine, D., Sessions, A., Eiler, J., 2015.
756 Distinguishing and understanding thermogenic and biogenic sources of methane using multiply
757 substituted isotopologues. Geochimica et Cosmochimica Acta 161, 219-247.

758 Taenzer, L., Labidi, J., Masterson, A.L., Feng, X., Rumble III, D., Young, E.D., Leavitt, W.D., 2020.
759 Low apparent $\Delta^{12}\text{CH}_2\text{D}_2$ in microbialgenic methane result from combinatorial isotope effects.
760 Geochimica et Cosmochimica Acta.

761 Van Mourik, T., & Van Duijneveldt, F. B. (1995). Ab initio calculations on the CH... O hydrogen-
762 bonded systems CH₄-H₂O, CH₃NH₂-H₂O and CH₃NH₃⁺-H₂O. *Journal of Molecular Structure:*
763 *THEOCHEM*, 341(1-3), 63-73.

764 Wang, D.T., Gruen, D.S., Lollar, B.S., Hinrichs, K.-U., Stewart, L.C., Holden, J.F., Hristov, A.N.,
765 Pohlman, J.W., Morrill, P.L., Könneke, M., 2015. Nonequilibrium clumped isotope signals in
766 microbial methane. Science 348, 428-431.

767 Wang, D.T., Reeves, E.P., McDermott, J.M., Seewald, J.S., Ono, S., 2018. Clumped isotopologue
768 constraints on the origin of methane at seafloor hot springs. Geochimica et Cosmochimica Acta
769 223, 141-158.

770 Wang, D.T., Sattler, A., Paccagnini, M., Chen, F.G., 2019. Method for calibrating methane clumped
771 isotope measurements via catalytic equilibration of methane isotopologues on γ -alumina. *Rapid*
772 *Communications in Mass Spectrometry*.
773 Welhan, J.A., 1988. Origins of methane in hydrothermal systems. *Chemical Geology* 71, 183-198.
774 Welhan, J.A., Craig, H., 1979. Methane and hydrogen in East Pacific Rise hydrothermal fluids.
775 *Geophysical Research Letters* 6, 829-831.
776 Whiticar, M.J., 1999. Carbon and hydrogen isotope systematics of bacterial formation and
777 oxidation of methane. *Chemical Geology* 161, 291-314.
778 Yeung, L.Y., 2016. Combinatorial effects on clumped isotopes and their significance in
779 biogeochemistry. *Geochimica et Cosmochimica Acta* 172, 22-38.
780 Young, E., Kohl, I., Lollar, B.S., Etiope, G., Rumble iii, D., Li, S., Haghnegahdar, M., Schauble, E.,
781 McCain, K., Foustoukos, D., 2017. The relative abundances of resolved $^{12}\text{CH}_2\text{D}_2$ and $^{13}\text{CH}_3\text{D}$ and
782 mechanisms controlling isotopic bond ordering in abiotic and biotic methane gases. *Geochimica*
783 *et Cosmochimica Acta* 203, 235-264.
784 Young, E.D., 2019. A Two-Dimensional Perspective on CH_4 Isotope Clumping: Distinguishing
785 Process from Source, in: Orcutt, B.N., Daniel, I., Dasgupta, R. (Eds.), *Deep Carbon: Past to Present*.
786 Cambridge University Press, Cambridge, pp. 388-414.
787